Physica E 70 (2015) 58–76

Contents lists available at ScienceDirect

Physica E

journal homepage: www.elsevier.com/locate/physe

Vibrations of double-nanotube systems with mislocation via a newly developed van der Waals model

Keivan Kiani *

Department of Civil Engineering, K.N. Toosi University of Technology, P.O. Box 15875-4416, Valiasr Ave., Tehran, Iran

HIGHLIGHTS

- Frequency analysis of doubly parallel SWCNT with arbitrary configuration is studied.
- A new continuum-based vdW force model is developed accounting for mislocation.
- Nonlocal shear deformable beams are employed and their equations are obtained.
- The limitations of the nonlocal Timoshenko beam are explained for various BCs.
- The roles of crucial factors on first five frequencies are explored comprehensively.

GRAPHICAL ABSTRACT

A general configuration of a system of doubly parallel SWCNTs. Frequency analysis of doubly parallel SWCNTs embedded in an elastic matrix is of highly interest. To this end, a powerful meshfree method is implemented to solve the integral-partial differential governing equations resulted from the nonlocal Timoshenko and higher-order beam theories.

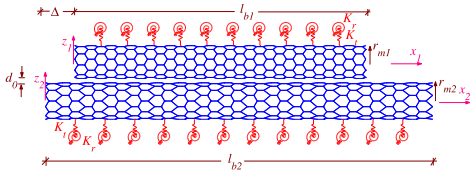

ARTICLE INFO

Article history:
Received 29 October 2014
Received in revised form
28 January 2015
Accepted 2 February 2015
Available online 3 February 2015

Keywords:
Transverse vibration
Doubly parallel single-walled carbon nanotubes
Van der Waals force
Reproducing kernel particle method
Nonlocal shear deformable beams
Mislocation effect

ABSTRACT

This study deals with transverse vibrations of two adjacent-parallel-mislocated single-walled carbon nanotubes (SWCNTs) under various end conditions. These tubes interact with each other and their surrounding medium through the intertube van der Waals (vdW) forces, and existing bonds between their atoms and those of the elastic medium. The elastic energy of such forces due to the deflections of nanotubes is appropriately modeled by defining a vdW force density function. In the previous works, vdW forces between two identical tubes were idealized by a uniform form of this function. The newly introduced function enables us to investigate the influences of both intertube free distance and longitudinal mislocation on the natural transverse frequencies of the nanosystem which consists of two dissimilar tubes. Such crucial issues have not been addressed yet, even for simply supported tubes. Using nonlocal Timoshenko and higher-order beam theories as well as Hamilton's principle, the strong form of the equations of motion is established. Seeking for an explicit solution to these integro-partial differential equations is a very problematic task. Thereby, an energy-based method in conjunction with an efficient meshfree method is proposed and the nonlocal frequencies of the elastically embedded nanosystem are determined. For simply supported nanosystems, the predicted first five frequencies of the proposed model are checked with those of assumed mode method, and a reasonably good agreement is achieved. Through various studies, the roles of the tube's length ratio, intertube free space, mislocation, small-scale effect, slenderness ratio, radius of SWCNTs, and elastic constants of the elastic matrix on the natural frequencies of the nanosystem with various end conditions are explained. The limitations of the nonlocal Timoshenko beam theory are also addressed. This work can be considered as a vital step towards better realizing of a more complex system that consists of vertically aligned SWCNTs of various lengths.

* Fax: +98 21 88779476.
E-mail addresses: k_kiani@kntu.ac.ir, keivankiani@yahoo.com

http://dx.doi.org/10.1016/j.physe.2015.02.002
1386-9477/

1. Introduction

The extraordinary physical, chemical, and mechanical properties of carbon nanotubes (CNTs) have attracted researchers from diverse range of fields to methodically explore their potential application in advanced technologies. To date, experimentally undertaken works have ensured the scientific communities that these newly synthesized materials can be efficiently used in drug and particle delivery systems [1–3], energy harvesting [4,5], nanoresonators [6–9], nanosensors (both physical and chemical) [10–12], and nano-/micro-electromechanical systems (NEMS/MEMS) [13–15]. In most of these applications, vibrations of CNTs play an important role and their dynamic mechanisms should be rationally understood. An individual single-walled carbon nanotube (SWCNT) is hard to believe to be employed for the above-mentioned purposes; however, ensembles of SWCNTs are commonly experimented to explore their efficiency for the considered jobs. This matter has been a driving force to investigate transverse vibrations of doubly parallel SWCNTs (DPSWCNTs) with an arbitrary configuration. Such a nanosystem can be imagined as the constitutive building block of vertically aligned ensembles of SWCNTs or as a simple constituent of even more complex systems such as haphazardly placed SWCNTs which are sometimes called jungles or forests of SWCNTs. As a result, a more rational modeling of such a nanosystem does not only increase our knowledge regarding their mechanical response, but also can be considered as a pivotal step towards better realizing of vibrations of more complex systems made of SWCNTs.

Due to the widely probable exploitations of CNTs and their composites, mechanical analysis and vibrations of individual SWCNTs have been extensively studied. For instance, free vibrations [16–18], vibrations due to moving nanoparticles [19–22], dynamic interactions with nanofluidics flow [23–25], mechanical sensing nano-objects [26–28] and unidirectional nanofluids [29], vibrations in the presence of magnetic fields [30–32], and their nonlinear vibrations [33–35] have been focus of attention for mechanical and structural engineers in recent years. Currently, free and forced vibrations of ensembles of SWCNTs have been examined via various nonlocal beam models [36–38]. Transverse vibrations of double-tube systems have been also examined [39,40], however, in the suggested models, the van der Waals (vdW) interactional forces between the atoms of two adjacent tubes were simply modeled by an elastic layer with one transverse constant. It implies that the role of the mislocation on dynamic response cannot be taken into account. These deficiencies and disabilities of the previously proposed models encouraged the author to revisit the problem in its most general vision, namely *doubly mislocated-parallel SWCNTs with arbitrary end conditions*. For this purpose, a novel model for evaluating the existing vdW force between two adjacent parallel tubes is suggested. In contrast to the past models in which the intertube vdW forces were considered by a constant, the present work suggests a more sophisticated model to capture such crucially interactional forces in which they play an important role in vibrations of such nanosystems. By this strategy, studying the role of mislocation on free vibration of the nanosystem is possible as it will be addressed comprehensively in the present work.

In most of the above-mentioned works, the vibrations of the nanosystems have been analyzed in the context of advanced theories of elasticity. It is chiefly related to this fact that at the atomic scale, vibration of each atom is influenced by the vibrations of its neighboring ones. Such a fact becomes crucial when the wavelength of the propagated waves is comparable with the atom bond length. Additionally, for bar-like or beam-like nanostructures when the ratio of the small-scale parameter to the nanostructure's length is not negligible, the classical theory of elasticity cannot capture the real or even near to exact vibration patterns of the nanostructure. These evidences are the most convincing reasons for exploiting advanced continuum mechanics to explore vibrations at the nanoscale. One of the most popular advanced theories is that developed by Eringen [41–43], called nonlocal continuum field theory. This theory explains that the state of stress or strain at each point of the continuum does not only depend on the stress or strain of that point, but also on the stresses or strains of its neighboring points. Such an issue is incorporated into the constitutive equations of the matter by a so-called small-scale factor. Generally, its magnitude is determined by comparing the obtained dispersion curves from the nonlocal model and those of a reliable atomic model. The magnitude of this parameter differs from one problem or matter to another one. Recent investigations [19,22] show that this parameter has a substantial effect on the mechanical behavior of stocky beam-like nanostructures. However, for slender nanosystems, its influence on their transverse dynamic response vanishes. In such a case, the discrepancies between the predicted results by the nonlocal model and those of the classical one would reduce.

In the present work, transverse vibration of DPSWCNTs in the context of the nonlocal continuum theory of Eringen is of interest. The most well-known shear deformable beam theories, namely Timoshenko [44,45] and higher-order of Reddy–Bickford [46,47], are adopted. Using Hamilton's principle, the equations of motion of the nanosystem at hand on the basis of these beam models are derived. An efficient numerical solution is suggested, and the natural frequencies of the nanosystem are obtained. The effects of nonlocality, various geometrical parameters associated with the nanosystem, and the interactions of the nanosystem with its surrounding elastic medium on the natural frequencies are comprehensively addressed.

2. Definition of the nanomechanical problem

Consider two parallel SWCNTs at the vicinity of each other. For mechanical modeling of such a system, each tube is replaced by an equivalent continuum structure (ECS). The ECS is a nano-scaled structure whose length and mean radius are identical to the length and radius of the parent tube, and its wall's thickness is 0.34 nm [48,49]. The intertube distance is denoted by d, the tubes lengths are l_{b_i}, their mean radii are r_{m_i}; $i = 1, 2$, their cross-section areas and moments inertia are denoted by A_{b_i} and I_{b_i}, respectively, and the mislocation of one tube with respect to the another one is represented by Δ (see Fig. 1). The mechanical properties of the ECSs are identified by the parameters ρ_{b_i}, E_{b_i}, G_{b_i}, and ν_{b_i} in which in order represent the density, Young's modulus, shear elastic moduli, and Poisson's ratio such that $G_{b_i} = E_{b_i}/2(1 + \nu_{b_i})$. Each tube interacts transversely and rotationally with its surrounding elastic medium. Such effects have been taken into account in modeling of the problem by a two-parameter elastic layer whose transverse and rotational stiffness are equal to K_t and K_r, respectively. Additionally, the nanotubes interact with each other due to the existing vdW forces between their constitutive atoms. Using nonlocal shear deformable beam theories, free transverse vibrations of such a nanosystem with various end conditions are of our interest.

For this purpose, a novel model for considering the intertube vdW forces is proposed in the next part. Subsequently, using Hamilton's principle, the strong form of the equations of motion of the elastically embedded nanosystem is obtained by establishing the models based on the nonlocal Timoshenko beam theory (NTBT) and the nonlocal higher-order beam theory (NHOBT).

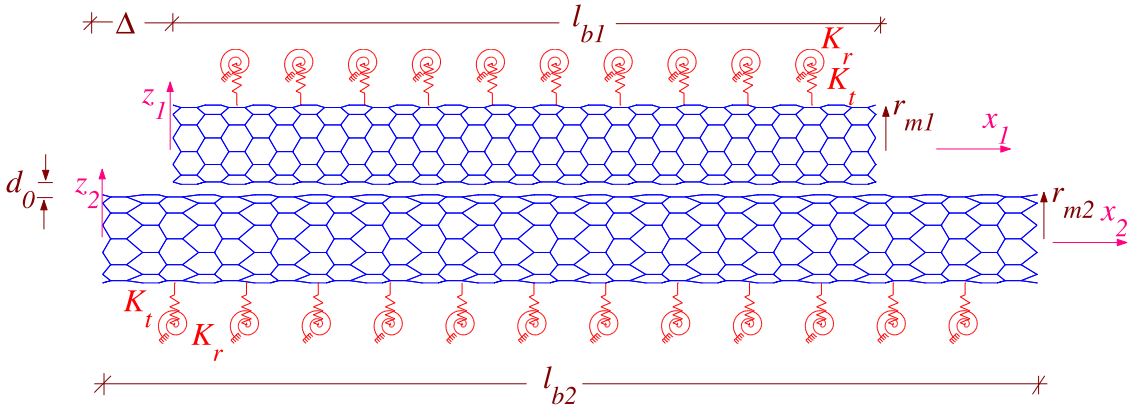

Fig. 1. A general configuration of the mislocated DPSWCNTs embedded in an elastic matrix and the considered coordinate systems.

3. A newly developed model for vdW forces

The interaction between two atoms of free of charge is commonly displayed by the L-J potential function [50], namely $\Phi(\lambda) = 4\epsilon[(\sigma/\lambda)^{12} - (\sigma/\lambda)^6]$ where λ, ϵ, and σ in order are the distance between two atoms, the potential well's depth, and the distance at which the potential function vanishes such that $\sigma = r_a/\sqrt[6]{2}$ in which r_a is the inter-atom distance at the equilibrium state. The vdW force between ith and jth atoms ($\mathbf{f}_{ij}$) is calculated by

$$\mathbf{f}_{ij} = -\frac{\mathrm{d}\Phi}{\mathrm{d}\lambda}\mathbf{e}_\lambda = \frac{24\epsilon}{\sigma^2}\left[2\left(\frac{\sigma}{\lambda}\right)^{14} - \left(\frac{\sigma}{\lambda}\right)^{8}\right]\vec{\lambda}, \tag{1}$$

where $\vec{\lambda}$ is the position vector of the jth atom with respect to the ith atom and its corresponding unit base vector is $\mathbf{e}_\lambda$. Since only transverse vibration of the nanosystem is of concern, the only displacement fields are as $w_i(x_i, t)$ where x_i is the longitudinal coordinate pertinent to the ith tube and t is the time parameter. Hence, the cylindrical coordinates of the walls of the transversely deformed nanotubes are stated by $(x_1, y_1 = r_{m_1}\cos\varphi_1, z_1 = r_{m_1}\sin\varphi_1 + w_1(x_1, t))$ and $(x_2, y_2 = r_{m_2}\cos\varphi_2, z_2 = r_{m_2}\sin\varphi_2 + w_2(x_2, t))$ where $0 \le x_i \le l_{b_i}$ and $0 \le \varphi_i \le 2\pi$; $i = 1, 2$. Additionally, d is the intertube distance such that $d = r_{m_1} + r_{m_2} + t_b + d_0$ where d_0 is the intertube free space (see Fig. 1). Therefore, the position vector would be

$$\vec{\lambda} = \left(x_2 - x_1 - \Delta\right)\mathbf{e}_{x_1} + \left(r_{m_2}\cos\varphi_2 - r_{m_1}\cos\varphi_1\right)\mathbf{e}_{y_1} + \left(d + r_{m_2}\sin\varphi_2 - r_{m_1}\sin\varphi_1 - \Delta w\right)\mathbf{e}_{z_1}, \tag{2}$$

where $\mathbf{e}_{x_1}$, $\mathbf{e}_{y_1}$, and $\mathbf{e}_{z_1}$ are the corresponding unit base vectors of the Cartesian coordinate system of the tube 1, $\Delta w = w_2 - w_1$. By introducing Eq. (2) to Eq. (1), the transverse component of the vdW force per unit square length of the ECSs due to their relative transverse motions along the z_1-axis is obtained as

$$f_z = \frac{24\epsilon\sigma_{CNT}^2}{\sigma^2}\int_0^{2\pi}\int_0^{2\pi}\left[2\left(\frac{\sigma}{\lambda}\right)^{14} - \left(\frac{\sigma}{\lambda}\right)^{8}\right]\left(r_{m_2}\sin\varphi_2 - r_{m_1}\sin\varphi_1 + d - \Delta w\right)\mathrm{d}\varphi_1\,\mathrm{d}\varphi_2, \tag{3}$$

where $\sigma_{CNT} = 4\sqrt{3}/9a^2$ is the surface density of the carbon atoms, and a denotes the carbon–carbon bond's length. Now Eq. (3) is approximated by expressing its Taylor expansion up to the first-order about the equilibrium state and the effect of higher-order terms is ignored. Thereby, the transverse vdW force per square lengths of the tubes due to their transverse motions is provided by

$$\Delta f_z = C_{vdW}(x_1, x_2)\Delta w, \tag{4}$$

in which

$$C_{vdW}(x_1, x_2; r_{m_1}, r_{m_2}, d) = -\frac{256\epsilon r_{m_1} r_{m_2}}{9a^4} \times \int_0^{2\pi}\int_0^{2\pi}\left\{\begin{array}{l}\sigma^{12}\left[\varrho^{-7} - 14\varrho^{-8}\left(d + r_{m_2}\sin\varphi_2 - r_{m_1}\sin\varphi_1\right)^2\right] - \\ \frac{\sigma^6}{2}\left[\varrho^{-4} - 8\varrho^{-5}\left(d + r_{m_2}\sin\varphi_2 - r_{m_1}\sin\varphi_1\right)^2\right]\end{array}\right\}\mathrm{d}\varphi_1\,\mathrm{d}\varphi_2, \tag{5a}$$

$$\varrho(x_1, x_2, \varphi_1, \varphi_2; r_{m_1}, r_{m_2}, d) = (x_1 + \Delta - x_2)^2 + \left(r_{m_2}\cos\varphi_2 - r_{m_1}\cos\varphi_1\right)^2 + \left(d + r_{m_2}\sin\varphi_2 - r_{m_1}\sin\varphi_1\right)^2, \tag{5b}$$

where C_{vdW} is called the vdW force density function. Additionally, the elastic energy resulted from the extra vdW interactional force is evaluated by

$$U_{vdW}(t) = \frac{1}{2}\int_{x_1=0}^{l_{b_1}}\int_{x_2=0}^{l_{b_2}} C_{vdW}(x_1, x_2)(\Delta w)^2\,\mathrm{d}x_1\,\mathrm{d}x_2. \tag{6}$$

4. Vibration analysis of elastically embedded DPSWCNTs using NTBT

4.1. Nonlocal equations of motion based on the NTBT

Based on the NTBT, the kinetic energy (T^T) and the strain energy of a nanosystem of elastically embedded DPSWCNTs (U^T) are given by

$$T^T = \frac{1}{2}\sum_{i=1}^{2}\int_0^{l_{b_i}}\rho_{b_i}\left(I_{b_i}\left(\dot{\theta}_i^T\right)^2 + A_{b_i}\left(\dot{w}_i^T\right)^2\right)\mathrm{d}x_i, \tag{7a}$$

$$U^T = \frac{1}{2}\sum_{i=1}^{2}\int_0^{l_{b_i}}\left(\begin{array}{l}-\theta_{i,x_i}^T\left(M_{b_i}^{nl}\right)^T + \left(w_{i,x_i}^T - \theta_i^T\right)\left(Q_{b_i}^{nl}\right)^T + \\ K_t\left(w_i^T\right)^2 + K_r\left(\theta_i^T\right)^2\end{array}\right)\mathrm{d}x_i + \frac{1}{2}\int_0^{l_{b_1}}\int_0^{l_{b_2}} C_{vdW}\left(w_2^T - w_1^T\right)^2\mathrm{d}x_1\,\mathrm{d}x_2, \tag{7b}$$

where $[\dot{\cdot}]$ and $[\cdot]_{,x_i}$ denote the first partial derivatives of $[\cdot]$ with respect to the time (t) and the spatial coordinate of the ith tube, respectively, $w_i^T = w_i^T(x_i, t)$, $\theta_i^T = \theta_i^T(x_i, t)$, $\left(Q_{b_i}^{nl}\right)^T = \left(Q_{b_i}^{nl}\right)^T(x_i, t)$, and $\left(M_{b_i}^{nl}\right)^T = \left(M_{b_i}^{nl}\right)^T(x_i, t)$ in order represent the transverse displacement, deformation angle, nonlocal shear force, and nonlocal bending moment of the ith tube, K_t and K_r are the transverse and rotational stiffness of the surrounding elastic matrix, respectively. According to the nonlocal continuum theory of Eringen [41,42], the nonlocal shear forces and the nonlocal bending moments of

the constitutive tubes of the nanosystem are expressed as [17,19]

$$\left(Q_{b_i}^{nl}\right)^T - (e_0a)_i^2\left(Q_{b_i}^{nl}\right)_{,x_ix_i}^T = k_{s_i}G_{b_i}A_{b_i}\left(w_{i,x_i}^T - \theta_i^T\right);\ i = 1, 2 \tag{8a}$$

$$\left(M_{b_i}^{nl}\right)^T - (e_0a)_i^2\left(M_{b_i}^{nl}\right)_{,x_ix_i}^T = -E_{b_i}I_{b_i}\theta_{i,x_i}^T, \tag{8b}$$

where $(e_0a)_i$ and k_{s_i} denote the small-scale parameter and shear correction factor of the ith nanotube. By employing Hamilton's principle at any time interval $[t_1, t_2]$, $\int_{t_1}^{t_2}\left(\delta T^T - \delta U^T\right)\mathrm{d}t = 0$ where δ is the variation symbol, the equations of motion of the nanosystem at hand in terms of the nonlocal forces within the tubes modeled based on the NTBT are derived as follows:

$$\rho_{b_i}I_{b_i}\ddot{\theta}_i^T - \left(Q_{b_i}^{nl}\right)^T + \left(M_{b_i}^{nl}\right)_{,x_i}^T + K_r\theta_i^T = 0;\ i = 1, 2, \tag{9a}$$

$$\rho_{b_i}A_{b_i}\ddot{w}_i^T - \left(Q_{b_i}^{nl}\right)_{,x_i}^T + \int_0^{\Lambda_i} C_{vdW}\left(w_1^T - w_2^T\right)\left(\delta_{i1} - \delta_{i2}\right)\mathrm{d}x_i + K_tw_i^T = 0. \tag{9b}$$

where δ_{ij} is the Kronecker delta tensor, and $\Lambda_i = \delta_{i2}l_{b_1} + \delta_{i1}l_{b_2}$. By introducing Eqs. (8a) and (8b) to Eqs. (9a) and (9b), the equations of motion of the elastically embedded DPSWCNTs in terms of deformation fields of the nanotubes are obtained as

$$\rho_{b_i}I_{b_i}\left(\ddot{\theta}_i^T - (e_0a)_i^2\ddot{\theta}_{i,x_ix_i}^T\right) - k_{s_i}G_{b_i}A_{b_i}\left(w_{i,x_i}^T - \theta_i^T\right) - E_{b_i}I_{b_i}\theta_{i,x_ix_i}^T + K_r\left(\theta_i^T - (e_0a)_i^2\theta_{i,x_ix_i}^T\right) = 0, \tag{10a}$$

$$\rho_{b_i}A_{b_i}\left(\ddot{w}_i^T - (e_0a)_i^2\ddot{w}_{i,x_ix_i}^T\right) - k_{s_i}G_{b_i}A_{b_i}\left(w_{i,x_ix_i}^T - \theta_{i,x_i}^T\right) + K_t\left(w_i^T - (e_0a)_i^2w_{i,x_ix_i}^T\right) + \int_0^{\Lambda_i} C_{vdW}\left(\left(w_1^T - w_2^T\right)\left(\delta_{i1} - \delta_{i2}\right) - (e_0a)_i^2w_{i,x_ix_i}^T\right)\mathrm{d}x_i = 0. \tag{10b}$$

To assess the problem in a more general context, the following dimensionless parameters are taken into account:

$$\tau = \frac{t}{l_{b_1}}\sqrt{\frac{k_{s_1}G_{b_1}}{\rho_{b_1}}},\quad \eta = \frac{E_{b_1}I_{b_1}}{k_{s_1}G_{b_1}A_{b_1}l_{b_1}^2},\quad \overline{w}_i^T = \frac{w_i^T}{l_{b_1}},\quad \overline{\theta}_i^T = \theta_i^T,\quad \varrho_4^2 = \frac{k_{s_2}G_{b_2}A_{b_2}}{k_{s_1}G_{b_1}A_{b_1}},$$
$$\overline{C}_{vdW}^T = \frac{C_{vdW}l_{b_1}^3}{k_{s_1}G_{b_1}A_{b_1}},\quad \overline{K}_r^T = \frac{K_r}{k_{s_1}G_{b_1}A_{b_1}},\quad \overline{K}_t^T = \frac{K_tl_{b_1}^2}{k_{s_1}G_{b_1}A_{b_1}},\quad \overline{\Lambda}_i = \delta_{i2} + \delta_{i1}\frac{l_{b_2}}{l_{b_1}},$$
$$\overline{\Gamma}_i = \delta_{i1} + \delta_{i2}\frac{l_{b_2}}{l_{b_1}}, \tag{11}$$

by introducing Eq. (11) to Eqs. (10a) and (10b), the dimensionless-nonlocal governing equations of an elastically embedded nanosystem with mislocated-parallel SWCNTs are derived as

$$\lambda_1^{-2}\varrho_2^{2i-2}\left(\overline{\theta}_{i,\tau\tau}^T - \mu_i^2\overline{\theta}_{i,\tau\tau\xi_i\xi_i}^T\right) - \varrho_4^{2i-2}\left(\overline{w}_{i,\xi_i}^T - \overline{\theta}_i^T\right) - \eta\varrho_3^{2i-2}\overline{\theta}_{i,\xi_i\xi_i}^T + \overline{K}_r^T\left(\overline{\theta}_i^T - \mu_i^2\overline{\theta}_{i,\xi_i\xi_i}^T\right) = 0, \tag{12a}$$

$$\varrho_1^{2i-2}\left(\overline{w}_{i,\tau\tau}^T - \mu_i^2\overline{w}_{i,\tau\tau\xi_i\xi_i}^T\right) - \varrho_4^{2i-2}\left(\overline{w}_{i,\xi_i\xi_i}^T - \overline{\theta}_{i,\xi_i}^T\right) + \int_0^{\overline{\Lambda}_i}\overline{C}_{vdW}^T\left(\left(\overline{w}_1^T - \overline{w}_2^T\right)\left(\delta_{i1} - \delta_{i2}\right) - \mu_i^2\overline{w}_{i,\xi_i\xi_i}^T\right) + \overline{K}_t^T\left(\overline{w}_i^T - \mu_i^2\overline{w}_{i,\xi_i\xi_i}^T\right) = 0. \tag{12b}$$

Eqs. (12a) and (12b) display four coupled integro-partial differential equations (IPDEs). Finding an explicit solution to these relations to analyze free transverse vibration of the nanosystem would not be an easy task anymore. In the upcoming part, a numerically based methodology is proposed and the natural frequencies are appropriately evaluated.

4.2. Application of RKPM to the governing equations

Let us premultiply Eqs. (12a) and (12b) by $\delta\overline{\theta}_i^T$ and $\delta\overline{w}_i^T$, and then integrate the sum of the resulting relations over the dimensionless spatial domains of the nanotubes. By applying the required integration by parts, it is obtainable:

$$\sum_{i=1}^{2}\int_0^{\overline{\Gamma}_i}\Big\{\lambda_1^{-2}\varrho_2^{2i-2}\left(\delta\overline{\theta}_i^T\overline{\theta}_{i,\tau\tau}^T + \mu_i^2\delta\overline{\theta}_{i,\xi_i}^T\overline{\theta}_{i,\tau\tau\xi_i}^T\right) - \varrho_4^{2i-2}\delta\overline{\theta}_i^T\left(\overline{w}_{i,\xi_i}^T - \overline{\theta}_i^T\right) + \varrho_1^{2i-2}\left(\delta\overline{w}_i^T\overline{w}_{i,\tau\tau}^T + \mu_i^2\delta\overline{w}_{i,\xi_i}^T\overline{w}_{i,\xi_i\tau\tau}^T\right) + \varrho_4^{2i-2}\delta\overline{w}_{i,\xi_i}^T\left(\overline{w}_{i,\xi_i}^T - \overline{\theta}_i^T\right) + \int_0^{\overline{\Lambda}_i}\overline{C}_{vdW}^T\delta\overline{w}_i^T\left(\left(\overline{w}_1^T - \overline{w}_2^T\right)\left(\delta_{i1} - \delta_{i2}\right) - \mu_i^2\overline{w}_{i,\xi_i\xi_i}^T\right)\mathrm{d}\xi_{3-i} + \eta\varrho_3^{2i-2}\delta\overline{\theta}_{i,\xi_i}^T\overline{\theta}_{i,\xi_i}^T + \overline{K}_r^T\left(\delta\overline{\theta}_i^T - \mu^2\delta\overline{\theta}_{i,\xi_i\xi_i}^T\right)\overline{\theta}_i^T + \overline{K}_t^T\left(\delta\overline{w}_i^T - \mu_i^2\delta\overline{w}_{i,\xi_i\xi_i}^T\right)\overline{w}_i^T\Big\}\mathrm{d}\xi_i = 0. \tag{13}$$

By adopting RKPM, the deformation fields of the nanotubes are spatially discretized as follows:

$$\overline{w}_i^T(\xi_i, \tau) = \sum_{I=1}^{\mathrm{NP}_i}\phi_I^{w_i}(\xi_i)\overline{w}_{i_I}^T(\tau),\quad \overline{\theta}_i^T(\xi_i, \tau) = \sum_{I=1}^{\mathrm{NP}_i}\phi_I^{\theta_i}(\xi_i)\overline{\theta}_{i_I}^T(\tau), \tag{14}$$

where $\phi_I^{w_i}$ and $\phi_I^{\theta_i}$ in order are the shape functions associated with the Ith RKPM's particle pertinent to the transverse displacement and rotation angle fields of the ith nanotube, $\overline{w}_{i_I}^T$ and $\overline{\theta}_{i_I}^T$ are their corresponding nodal parameter values, and NP_i is the number of RKPM's particles associated with the deformation fields of the ith nanotube. By substituting Eq. (14) into Eq. (13), one can arrive to the following set of $2\times(\mathrm{NP}_1 + \mathrm{NP}_2)$ second-order ordinary differential equations (ODEs):

$$\begin{bmatrix} [\overline{\mathbf{M}}_b^T]^{\theta_1\theta_1} & [\overline{\mathbf{M}}_b^T]^{\theta_1w_1} & [\overline{\mathbf{M}}_b^T]^{\theta_1\theta_2} & [\overline{\mathbf{M}}_b^T]^{\theta_1w_2} \\ [\overline{\mathbf{M}}_b^T]^{w_1\theta_1} & [\overline{\mathbf{M}}_b^T]^{w_1w_1} & [\overline{\mathbf{M}}_b^T]^{w_1\theta_2} & [\overline{\mathbf{M}}_b^T]^{w_1w_2} \\ [\overline{\mathbf{M}}_b^T]^{\theta_2\theta_1} & [\overline{\mathbf{M}}_b^T]^{\theta_2w_1} & [\overline{\mathbf{M}}_b^T]^{\theta_2\theta_2} & [\overline{\mathbf{M}}_b^T]^{\theta_2w_2} \\ [\overline{\mathbf{M}}_b^T]^{w_2\theta_1} & [\overline{\mathbf{M}}_b^T]^{w_2w_1} & [\overline{\mathbf{M}}_b^T]^{w_2\theta_2} & [\overline{\mathbf{M}}_b^T]^{w_2w_2} \end{bmatrix}\begin{Bmatrix} \overline{\boldsymbol{\theta}}_{1,\tau\tau}^T \\ \overline{\mathbf{w}}_{1,\tau\tau}^T \\ \overline{\boldsymbol{\theta}}_{2,\tau\tau}^T \\ \overline{\mathbf{w}}_{2,\tau\tau}^T \end{Bmatrix} + \begin{bmatrix} [\overline{\mathbf{K}}_b^T]^{\theta_1\theta_1} & [\overline{\mathbf{K}}_b^T]^{\theta_1w_1} & [\overline{\mathbf{K}}_b^T]^{\theta_1\theta_2} & [\overline{\mathbf{K}}_b^T]^{\theta_1w_2} \\ [\overline{\mathbf{K}}_b^T]^{w_1\theta_1} & [\overline{\mathbf{K}}_b^T]^{w_1w_1} & [\overline{\mathbf{K}}_b^T]^{w_1\theta_2} & [\overline{\mathbf{K}}_b^T]^{w_1w_2} \\ [\overline{\mathbf{K}}_b^T]^{\theta_2\theta_1} & [\overline{\mathbf{K}}_b^T]^{\theta_2w_1} & [\overline{\mathbf{K}}_b^T]^{\theta_2\theta_2} & [\overline{\mathbf{K}}_b^T]^{\theta_2w_2} \\ [\overline{\mathbf{K}}_b^T]^{w_2\theta_1} & [\overline{\mathbf{K}}_b^T]^{w_2w_1} & [\overline{\mathbf{K}}_b^T]^{w_2\theta_2} & [\overline{\mathbf{K}}_b^T]^{w_2w_2} \end{bmatrix}\begin{Bmatrix} \overline{\boldsymbol{\theta}}_1^T \\ \overline{\mathbf{w}}_1^T \\ \overline{\boldsymbol{\theta}}_2^T \\ \overline{\mathbf{w}}_2^T \end{Bmatrix} = \begin{Bmatrix} \mathbf{0} \\ \mathbf{0} \\ \mathbf{0} \\ \mathbf{0} \end{Bmatrix}, \tag{15}$$

where the nonzero vectors and matrices in Eq. (15) are given in Appendix A.1.

4.3. Enforcing the boundary conditions and evaluating the natural frequencies

Without loss of generality, we restrict our analysis to nanosystems with simply supported ends (SS), fully clamped ends (CC), and cantilevered tubes (CF). The boundary conditions of these nanosystems are expressed by

$$\begin{aligned} &\text{SS:}\quad \overline{w}_i^T(0,\tau) = \overline{w}_i^T(\overline{\Gamma}_i,\tau) = 0;\quad \left(\overline{M}_{b_i}^{nl}\right)^T(0,\tau) = \left(\overline{M}_{b_i}^{nl}\right)^T(\overline{\Gamma}_i,\tau) = 0;\ i = 1, 2,\\ &\text{CC:}\quad \overline{w}_i^T(0,\tau) = \overline{w}_i^T(\overline{\Gamma}_i,\tau) = 0;\quad \overline{\theta}_i^T(0,\tau) = \overline{\theta}_i^T(\overline{\Gamma}_i,\tau) = 0,\\ &\text{CF:}\quad \overline{w}_i^T(0,\tau) = \overline{\theta}_i^T(0,\tau) = 0;\quad \left(\overline{M}_{b_i}^{nl}\right)^T(\overline{\Gamma}_i,\tau) = \left(\overline{Q}_{b_i}^{nl}\right)^T(\overline{\Gamma}_i,\tau) = 0. \end{aligned} \tag{16}$$

In order to impose the essential boundary conditions of Eq. (16), the corrected collocation method [51] is implemented. After adopting this approach, one can arrive to a new set of second-order ODEs. By considering a harmonic form for the time-dependent vector of such a set of equations, then by solving the resulting set of eigenvalue equations, the natural frequencies of the elastically embedded DPSWCNTs based on the NTBT would be readily evaluated.

5. Vibration analysis of elastically embedded DPSWCNTs using NHOBT

5.1. Nonlocal equations of motion based on the NHOBT

In the framework of the NHOBT, the kinetic energy (T^H) and the energy of elastically embedded DPSWCNTs embedded in an elastic matrix (U^H) are expressed by

$$T^H=\frac{1}{2}\sum_{i=1}^{2}\int_0^{l_{b_i}}\begin{pmatrix} I_{0_i}\left(\dot{w}_{i,x_i}^H\right)^2+I_{2_i}\left(\dot{\psi}_i^H\right)^2+\alpha_i^2 I_{6_i}\left(\dot{\psi}_i^H+\dot{w}_{i,x_i}^H\right)^2 \\ -2\alpha_i I_{4_i}\dot{\psi}_i^H\left(\dot{\psi}_i^H+\dot{w}_{i,x_i}^H\right)\end{pmatrix}\mathrm{d}x_i, \tag{17a}$$

$$U^H=\frac{1}{2}\sum_{i=1}^{2}\int_0^{l_{b_i}}\begin{pmatrix}\left(\psi_i^H+w_{i,x_i}^H\right)\left(\alpha_i\left(P_{b_i}^{nl}\right)_{,x_i}^H+\left(Q_{b_i}^{nl}\right)^H\right)+ \\ +\psi_{i,x_i}^H\left(M_{b_i}^{nl}\right)^H+K_r\left(\psi_i^H\right)^2+K_t\left(w_i^H\right)^2\end{pmatrix}\mathrm{d}x_i$$
$$+\frac{1}{2}\int_0^{l_{b1}}\int_0^{l_{b2}}C_{vdW}\left(w_2^H-w_1^H\right)^2\mathrm{d}x_1\,\mathrm{d}x_2, \tag{17b}$$

where $w_i^H=w_i^H(x_i,t)$, $\psi_i^H=\psi_i^H(x_i,t)$, $\left(M_{b_i}^{nl}\right)^H=\left(M_{b_i}^{nl}\right)^H(x_i,t)$, and $\left(Q_{b_i}^{nl}\right)^H=\left(Q_{b_i}^{nl}\right)^H(x_i,t)$ denote the transverse displacement, angle of deflection, nonlocal bending moment, and nonlocal shear force of the ith tube in which modeled based on the NHOBT, respectively. In the context of the nonlocal theory of elasticity of Eringen [41,42], these nonlocal forces are related to their local counterparts as follows [19,21,52]:

$$M_{b_i}^H-(e_0a)_i^2M_{b_i,x_ix_i}^H=J_{2_i}\psi_{i,x_i}^H-\alpha_iJ_{4_i}\left(\psi_{i,x_i}^H+w_{i,x_ix_i}^H\right);\quad i=1,2, \tag{18a}$$

$$\left(Q_{b_i}^H+\alpha_iP_{b_i,x_i}^H\right)-(e_0a)_i^2\left(Q_{b_i}^H+\alpha_iP_{b_i,x_i}^H\right)_{,x_ix_i}$$
$$=\kappa_i\left(\psi_i^H+w_{i,x_i}^H\right)+\alpha_iJ_{4_i}\psi_{i,x_ix_i}^H-\alpha_i^2J_{6_i}\left(\psi_{i,x_ix_i}^H+w_{i,x_ix_ix_i}^H\right), \tag{18b}$$

where

$$\alpha_i=1/(3r_{o_i}^2);\quad i=1,2,$$
$$\kappa_i=\int_{A_{b_i}}G_{b_i}(1-3\alpha_iz^2)\,\mathrm{d}A,$$
$$I_{n_i}=\int_{A_{b_i}}\rho_{b_i}z^n\,\mathrm{d}A;\quad n=0,2,4,6,$$
$$J_{n_i}=\int_{A_{b_i}}E_{b_i}z^n\,\mathrm{d}A;\quad n=2,4,6. \tag{19}$$

By employing Hamilton's principle in view of Eqs. (17a) and (17b), the equations of motion of DOSWCNTs embedded in an elastic matrix in terms of the nonlocal internal forces are constructed as

$$\left(I_{2_i}-2\alpha_iI_{4_i}+\alpha_i^2I_{6_i}\right)\ddot{\psi}_i^H+\left(\alpha_i^2I_{6_i}-\alpha_iI_{4_i}\right)\ddot{w}_{i,x_i}^H$$
$$+\left(Q_{b_i}^{nl}\right)^H+\alpha_i\left(P_{b_i}^{nl}\right)_{,x_i}^H-\left(M_{b_i}^{nl}\right)_{,x_i}^H+K_r\psi_i^H=0;\quad i=1,2, \tag{20a}$$

$$I_{0_i}\ddot{w}_i^H-\left(\alpha_i^2I_{6_i}-\alpha_iI_{4_i}\right)\ddot{\psi}_{2,x_i}^H-\alpha_i^2I_{6_i}\ddot{w}_{2,x_ix_i}^H-\left(Q_{b_i}^{nl}\right)_{,x_i}^H-\alpha_i\left(P_{b_i}^{nl}\right)_{,x_ix_i}^H$$
$$+\int_0^{\Lambda_i}C_{vdW}\left(w_1^H-w_2^H\right)\left(\delta_{i1}-\delta_{i2}\right)\mathrm{d}\xi_{3-i}+K_tw_i^H=0, \tag{20b}$$

by introducing Eqs. (18a) and (18b) to Eqs. (20a) and (20b), the nonlocal equations of motion of the considered nanosystem in terms of deformation fields are obtained as

$$\left(I_{2_i}-2\alpha_iI_{4_i}+\alpha_2^2I_{6_i}\right)\left(\ddot{\psi}_i^H-(e_0a)_i^2\ddot{\psi}_{i,x_ix_i}^H\right)$$
$$+\left(\alpha_i^2I_{6_i}-\alpha_iI_{4_i}\right)\left(\ddot{w}_{i,x_i}^H-(e_0a)_i^2\ddot{w}_{i,x_ix_ix_i}^H\right)-\left(\alpha_i^2J_{6_i}-\alpha_iJ_{4_i}\right)$$
$$w_{i,x_ix_ix_i}^H-\left(J_{2_i}-2\alpha J_{4_i}+\alpha_i^2J_{6_i}\right)\psi_{i,x_ix_i}^H+K_r\left(\psi_i^H-(e_0a)_i^2\psi_{i,x_ix_i}^H\right)$$
$$=0, \tag{21a}$$

$$I_{0_i}\left(\dot{w}_i^H-(e_0a)_i^2\dot{w}_{i,x_ix_i}^H\right)-\left(\alpha_i^2I_{6_i}-\alpha_iI_{4_i}\right)\left(\dot{\psi}_{i,x_i}^H-(e_0a)_i^2\dot{\psi}_{i,x_ix_ix_i}^H\right)$$
$$-\alpha_i^2I_{6_i}\left(\dot{w}_{i,x_ix_i}^H-(e_0a)_i^2\dot{w}_{i,x_ix_ix_ix_i}^H\right)-\kappa_i\left(\psi_{i,x_i}^H+w_{i,x_ix_i}^H\right)+\left(\alpha_i^2J_{6_i}-\alpha_iJ_{4_i}\right)\psi_{i,x_ix_ix_i}^H$$
$$+\int_0^{\Lambda_i}C_{vdW}\left(\left(w_1^H-w_2^H\right)\left(\delta_{i1}-\delta_{i2}\right)-(e_0a)_i^2w_{i,x_ix_i}^H\right)\mathrm{d}\xi_{3-i}$$
$$+\alpha_i^2J_{6_i}w_{i,x_ix_ix_ix_i}^H+K_t\left(w_i^H-(e_0a)_i^2w_{i,x_ix_i}^H\right)=0;\quad i=1,2. \tag{21b}$$

For a more rational investigation of the problem at hand, the following dimensionless parameters are considered:

$$\tau=\frac{\alpha_1}{l_{b1}^2}\sqrt{\frac{J_{6_1}}{I_{0_1}}}t,\quad \overline{w}_i^H=\frac{w_i^H}{l_b},\ \overline{\psi}_i^H=\psi_i^H,\quad \overline{C}_{vdW}^H=\frac{C_{vdW}\,l_{b1}^5}{\alpha_1^2J_{6_1}},$$
$$\vartheta_1^2=\frac{I_{0_2}}{I_{0_1}},\quad \vartheta_2^2=\frac{\alpha_2J_{4_2}-\alpha_2^2I_{6_2}}{\alpha_1J_{4_1}-\alpha_1^2I_{6_1}},\quad \vartheta_3^2=\frac{\alpha_2^2I_{6_2}}{\alpha_1^2I_{6_1}},\quad \vartheta_4^2=\frac{\kappa_2}{\kappa_1},\quad \vartheta_5^2=\frac{\alpha_2J_{4_2}-\alpha_2^2J_{6_2}}{\alpha_1J_{4_1}-\alpha_1^2J_{6_1}},$$
$$\vartheta_6^2=\frac{\alpha_2^2J_{6_2}}{\alpha_1^2J_{6_1}},\quad \vartheta_7^2=\frac{I_{2_2}-2\alpha_2I_{4_2}+\alpha_2^2I_{6_2}}{I_{2_1}-2\alpha_1I_{4_1}+\alpha_1^2I_{6_1}},\quad \vartheta_8^2=\frac{J_{2_2}-2\alpha_2J_{4_2}+\alpha_2^2J_{6_2}}{J_{2_1}-2\alpha_1J_{4_1}+\alpha_1^2J_{6_1}},$$
$$\gamma_1^2=\frac{\alpha_1I_{4_1}-\alpha_1^2I_{6_1}}{I_{0_1}l_b^2},\quad \gamma_2^2=\frac{\alpha_1^2I_{6_1}}{I_{0_1}l_{b1}^2},\quad \gamma_3^2=\frac{\kappa_1l_{b1}^2}{\alpha_1^2J_{6_1}},\quad \gamma_4^2=\frac{\alpha_1J_{4_1}-\alpha_1^2J_{6_1}}{\alpha_1^2J_{6_1}},$$
$$\gamma_6^2=\frac{\alpha_1I_{4_1}-\alpha_1^2I_{6_1}}{I_{2_1}-2\alpha_1I_{4_1}+\alpha_1^2I_{6_1}},\quad \gamma_7^2=\frac{\kappa_1I_{0_1}l_{b1}^4}{\alpha_1^2J_{6_1}(I_{2_1}-2\alpha_1I_{4_1}+\alpha_1^2I_{6_1})},$$
$$\gamma_8^2=\frac{(J_{2_1}-2\alpha_1J_{4_1}+\alpha_1^2J_{6_1})I_{0_1}l_{b1}^2}{\alpha_1^2J_{6_1}(I_{2_1}-2\alpha_1I_{4_1}+\alpha_1^2I_{6_1})},\quad \gamma_9^2=\frac{(\alpha_1J_{4_1}-\alpha_1^2J_{6_1})I_{0_1}l_{b1}^2}{\alpha_1^2J_{6_1}(I_{2_1}-2\alpha_1I_{4_1}+\alpha_1^2I_{6_1})},$$
$$\overline{K}_t^H=\frac{K_tI_{0_1}l_{b1}^4}{\alpha_1^2J_{6_1}},\quad \overline{K}_r^H=\frac{K_rI_{0_1}l_{b1}^4}{\alpha_1^2(I_{2_1}-2\alpha_1I_{4_1}+\alpha_1^2I_{6_1})J_{6_1}}. \tag{22}$$

By introducing Eq. (22) to Eqs. (21a) and (21b), the dimensionless-nonlocal governing equations of free transverse vibration of DPSWCNTs embedded in an elastic matrix on the basis of the NHOBT are obtained as

$$\vartheta_7^{2i-2}\left(\overline{\psi}_{i,\tau\tau}^H-\mu_i^2\overline{\psi}_{i,\xi_i^2\xi_i^2\tau\tau}^H\right)-\vartheta_2^{2i-2}\gamma_6^2(\overline{w}_{i,\tau\tau\xi_i}^H-\mu_i^2\overline{w}_{i,\tau\tau\xi_i^2\xi_i^2\xi_i}^H)$$
$$+\vartheta_4^{2i-2}\gamma_7^2(\overline{\psi}_i^H+\overline{w}_{i,\xi_i}^H)\quad-\vartheta_8^{2i-2}\gamma_8^2\overline{\psi}_{i,\xi_i^2\xi_i}^H+\vartheta_5^2\gamma_9^2\overline{w}_{i,\xi_i^2\xi_i^2\xi_i}^H$$
$$+\overline{K}_r^H\left(\overline{\psi}_i^H-\mu_i^2\overline{\psi}_{i,\xi_i^2\xi_i}^H\right)=0, \tag{23a}$$

$$\vartheta_1^{2i-2}(\overline{w}_{i,\tau\tau}^H-\mu_i^2\overline{w}_{i,\tau\tau\xi_i^2\xi_i}^H)+\vartheta_2^{2i-2}\gamma_1^2\left(\overline{\psi}_{i,\tau\tau\xi_i}^H-\mu_i^2\overline{\psi}_{i,\tau\tau\xi_i^2\xi_i^2\xi_i}^H\right)\vartheta_5^{2i-2}\gamma_4^2\overline{\psi}_{i,\xi_i^2\xi_i^2\xi_i}^H$$
$$+\vartheta_6^{2i-2}\overline{w}_{i,\xi_i^2\xi_i^2\xi_i^2\xi_i}^H-\vartheta_3^{2i-2}\gamma_2^2(\overline{w}_{i,\tau\tau\xi_i^2\xi_i}^H-\mu_i^2\overline{w}_{i,\tau\tau\xi_i^2\xi_i^2\xi_i^2\xi_i}^H)-\vartheta_4^{2i-2}\gamma_3^2(\overline{\psi}_{i,\xi}^H+\overline{w}_{i,\xi_i^2\xi_i}^H)$$
$$-\int_0^{\Lambda_i}\overline{C}_{vdW}^H\left(\left(\overline{w}_1^H-\overline{w}_2^H\right)\left(\delta_{i1}-\delta_{i2}\right)-\mu_i^2\overline{w}_{i,\xi_i^2\xi_i}^H\right)\mathrm{d}\xi_i$$
$$+\overline{K}_t^H\left(\overline{w}_i^H-\mu_i^2\overline{w}_{i,\xi_i^2\xi_i}^H\right)=0;\quad i=1,2. \tag{23b}$$

From mathematical point of view, Eqs. (23a) and (23b) describe four coupled IPDEs in which seeking an analytical solution to them is a very problematic task. As an alternative approach, an efficient meshless method is proposed in the following part.

5.2. Application of RKPM to the governing equations

Application of the RKPM for discretization of the unknown fields in Eqs. (23a) and (23b) is of concern. To this end, these equations in order are multiplied by $\delta\overline{\psi}_i^H$ and $\delta\overline{w}_i^H$. By taking the integral of the sum of the resulting expressions over the dimensionless spatial domains of the nanotubes, and then applying the required integration by parts, one can arrive at the following relation:

$$\begin{aligned}
&\sum_{i=1}^{2}\int_0^{\overline{\Gamma}_i}\Big\{\vartheta_7^{2i-2}\Big(\delta\overline{\psi}_i^H\overline{\psi}_{i,\tau\tau}^H+\mu_i{}^2\delta\overline{\psi}_{i,\xi_i}^H\overline{\psi}_{i,\xi_i\tau\tau}^H\Big)\\
&-\vartheta_2^{2i-2}\gamma_6^2\Big(\delta\overline{\psi}_i^H\overline{w}_{i,\xi_i\tau\tau}^H-\mu_i{}^2\delta\overline{\psi}_{i,\xi_i}^H\overline{w}_{i,\xi_i\xi_i\tau\tau}^H\Big)\\
&+\vartheta_4^{2i-2}\gamma_7^2\delta\overline{\psi}_i^H\Big(\overline{\psi}_i^H+\overline{w}_{i,\xi_i}^H\Big)+\vartheta_8^{2i-2}\gamma_8^2\delta\overline{\psi}_{i,\xi_i}^H\overline{\psi}_{i,\xi_i}^H\\
&-\vartheta_5^{2i-2}\gamma_9^2\delta\overline{\psi}_{i,\xi_i}^H\overline{w}_{i,\xi_i\xi_i}^H+\vartheta_1^{2i-2}\Big(\delta\overline{w}_i^H\overline{w}_{i,\tau\tau}^H+\mu^2\delta\overline{w}_{i,\xi_i}^H\overline{w}_{i,\xi_i\tau\tau}^H\Big)\\
&-\vartheta_2^{2i-2}\gamma_1^2\Big(\delta\overline{w}_{i,\xi_i}^H\overline{\psi}_{i,\tau\tau}^H+\mu_i{}^2\delta\overline{w}_{i,\xi_i\xi_i}^H\overline{\psi}_{i,\xi_i\tau\tau}^H\Big)\\
&+\vartheta_3^{2i-2}\gamma_2^2\Big(\delta\overline{w}_{i,\xi_i}^H\overline{w}_{i,\xi_i\tau\tau}^H+\mu_i{}^2\delta\overline{w}_{i,\xi_i\xi_i}^H\overline{w}_{i,\xi_i\xi_i\tau\tau}^H\Big)\\
&+\vartheta_4^{2i-2}\gamma_3^2\delta\overline{w}_{i,\xi_i}^H\Big(\overline{\psi}_i^H+\overline{w}_{i,\xi_i}^H\Big)-\vartheta_5^{2i-2}\gamma_4^2\delta\overline{w}_{i,\xi_i\xi_i}^H\overline{\psi}_{i,\xi_i}^H\\
&+\vartheta_6^{2i-2}\delta\overline{w}_{i,\xi_i\xi_i}^H\overline{w}_{i,\xi_i\xi_i}^H\\
&+\int_0^{\overline{\Gamma}_i}\overline{C}_{vdW}^H\delta\overline{w}_i^H\Big(\big(\overline{w}_1^H-\overline{w}_2^H\big)\big(\delta_{i1}-\delta_{i2}\big)-\mu_i\overline{w}_{i,\xi_i\xi_i}^H\Big)\,\mathrm{d}\xi_{3-i}\\
&+\overline{K}_r^H\Big(\delta\overline{\psi}_i^H-\mu_i{}^2\delta\overline{\psi}_{i,\xi_i\xi_i}^H\Big)\overline{\psi}_i^H+\overline{K}_t^H\Big(\delta\overline{w}_i^H-\mu_i{}^2\delta\overline{w}_{i,\xi_i\xi_i}^H\Big)\overline{w}_i^H\Big\}\,\mathrm{d}\xi_i\\
&=0.
\end{aligned}\tag{24}$$

By adopting RKPM, the transverse and angle of rotation fields of the nanotubes are expressed by

$$\overline{w}_i^H(\xi_i,\tau)=\sum_{I=1}^{NP_i}\phi_I^{w_i}(\xi_i)\overline{w}_{i_I}^H(\tau),\quad \overline{\psi}_i^H(\xi_i,\tau)=\sum_{I=1}^{NP_i}\phi_I^{\psi_i}(\xi_i)\overline{\psi}_{i_I}^H(\tau),\tag{25}$$

by substituting Eq. (25) into Eq. (24), the following set of ordinary differential equations is derived:

$$\begin{aligned}
&\begin{bmatrix}
[\overline{\mathbf{M}}_b^H]^{\psi_1\psi_1} & [\overline{\mathbf{M}}_b^H]^{\psi_1 w_1} & [\overline{\mathbf{M}}_b^H]^{\psi_1\psi_2} & [\overline{\mathbf{M}}_b^H]^{\psi_1 w_2}\\
[\overline{\mathbf{M}}_b^H]^{w_1\psi_1} & [\overline{\mathbf{M}}_b^H]^{w_1 w_1} & [\overline{\mathbf{M}}_b^H]^{w_1\psi_2} & [\overline{\mathbf{M}}_b^H]^{w_1 w_2}\\
[\overline{\mathbf{M}}_b^H]^{\psi_2\psi_1} & [\overline{\mathbf{M}}_b^H]^{\psi_2 w_1} & [\overline{\mathbf{M}}_b^H]^{\psi_2\psi_2} & [\overline{\mathbf{M}}_b^H]^{\psi_2 w_2}\\
[\overline{\mathbf{M}}_b^H]^{w_2\psi_1} & [\overline{\mathbf{M}}_b^H]^{w_2 w_1} & [\overline{\mathbf{M}}_b^H]^{w_2\psi_2} & [\overline{\mathbf{M}}_b^H]^{w_2 w_2}
\end{bmatrix}
\begin{Bmatrix}\overline{\Psi}_{1,\tau\tau}^H\\ \overline{\mathbf{w}}_{1,\tau\tau}^H\\ \overline{\Psi}_{2,\tau\tau}^H\\ \overline{\mathbf{w}}_{2,\tau\tau}^H\end{Bmatrix}\\
&+\begin{bmatrix}
[\overline{\mathbf{K}}_b^H]^{\psi_1\psi_1} & [\overline{\mathbf{K}}_b^H]^{\psi_1 w_1} & [\overline{\mathbf{K}}_b^H]^{\psi_1\psi_2} & [\overline{\mathbf{K}}_b^H]^{\psi_1 w_2}\\
[\overline{\mathbf{K}}_b^H]^{w_1\psi_1} & [\overline{\mathbf{K}}_b^H]^{w_1 w_1} & [\overline{\mathbf{K}}_b^H]^{w_1\psi_2} & [\overline{\mathbf{K}}_b^H]^{w_1 w_2}\\
[\overline{\mathbf{K}}_b^H]^{\psi_2\psi_1} & [\overline{\mathbf{K}}_b^H]^{\psi_2 w_1} & [\overline{\mathbf{K}}_b^H]^{\psi_2\psi_2} & [\overline{\mathbf{K}}_b^H]^{\psi_2 w_2}\\
[\overline{\mathbf{K}}_b^H]^{w_2\psi_1} & [\overline{\mathbf{K}}_b^H]^{w_2 w_1} & [\overline{\mathbf{K}}_b^H]^{w_2\psi_2} & [\overline{\mathbf{K}}_b^H]^{w_2 w_2}
\end{bmatrix}
\begin{Bmatrix}\overline{\Psi}_1^H\\ \overline{\mathbf{w}}_1^H\\ \overline{\Psi}_2^H\\ \overline{\mathbf{w}}_2^H\end{Bmatrix}
=\begin{Bmatrix}\mathbf{0}\\ \mathbf{0}\\ \mathbf{0}\\ \mathbf{0}\end{Bmatrix}.
\end{aligned}\tag{26}$$

where the nonzero vectors and matrices in Eq. (26) are provided in Appendix A.2.

5.3. Enforcing the boundary conditions and evaluating the natural frequencies

For SS, CC, and CF boundary conditions, the following relations should be satisfied:

$$\begin{aligned}
&\text{SS:}\quad \overline{w}_i^H(0,\tau)=\overline{w}_i^H(\overline{\Gamma}_i,\tau)=0;\quad \Big(\overline{M}_{b_i}^{nl}\Big)^H(0,\tau)=\Big(\overline{M}_{b_i}^{nl}\Big)^H(\overline{\Gamma}_i,\tau)=0;\quad i=1,2,\\
&\text{CC:}\quad \overline{w}_i^H(0,\tau)=\overline{w}_i^H(\overline{\Gamma}_i,\tau)=0;\ \overline{\theta}_i^H(0,\tau)=\overline{\theta}_i^H(\overline{\Gamma}_i,\tau)=0,\\
&\text{CF:}\ \overline{w}_i^H(0,\tau)=\overline{\theta}_i^H(0,\tau)=0;\quad \Big(\overline{M}_{b_i}^{nl}\Big)^H(\overline{\Gamma}_i,\tau)=\Big(\Big(\overline{Q}_{b_i}^{nl}\Big)^H+\alpha_i\Big(\overline{P}_{b_i}^{nl}\Big)^H\Big)(\overline{\Gamma}_i,\tau)=0.
\end{aligned}\tag{27}$$

To apply the boundary conditions in Eq. (27) and to evaluate the natural frequencies of the nanosystem, the similar methodologies mentioned in Section 4.3 are followed.

6. Results and discussion

Consider elastically embedded DPSWCNTs with the following data: $E_{b_1}=E_{b_2}=1$ TPa, $\nu_1=\nu_2=0.2$, $\rho_{b_1}=\rho_{b_2}=2300\ \mathrm{kg/m^3}$, $r_{m_1}=r_{m_2}=1.5$ nm. In the performed investigations, the intertube distance is evaluated by $d=r_{m_1}+r_{m_2}+1.5t_b$, the mislocation is provoked (i.e., $\Delta=0$) and the interactions of the nanosystem with the surrounding elastic matrix have been ignored (i.e., $K_t=K_r=0$), except their values have been explicitly specified. In all RKPM calculations pertinent to each unknown field, 21 uniform particles within the spatial domain of each tube have been taken into account (i.e., $NP_1=NP_2=21$). For evaluating the RKPM's shape function, linear base function, cubic spline window function, and 6 Gaussian points in each direction of the computational cell have been used. The dilation parameter is set equal to 3.2 times of the inter-particle distance.

In the following parts, a comparison study is performed in a special case to ensure regarding the accuracy of calculations of the RKPM. Thereafter, a comprehensive parametric study is presented to examine the roles of the influential factors on the free dynamic response of the elastically embedded nanosystem.

6.1. Some verification studies

In order to ensure about the exactness of the carried out calculations by the proposed models, the predicted free transverse vibration of the nanosystem up to the fifth vibration mode is checked with those of another numerical method for a particular case. To this end, for the nanosystem with simply supported ends, assumed mode method (AMM) is employed as an alternative methodology for discretizing the known fields pertinent to the NTBT and NHOBT (see Appendix B). In Table 1, the predicted first five natural frequencies of the nanosystem by the RKPM and AMM based on the NTBT and NHOBT for various levels of the small-scale parameter and slenderness ratio have been provided. The results are given for a nanosystem which is not in contact with the elastic matrix (i.e., $K_t=K_r=0$) and the double identical tubes are exactly placed in front of each other (i.e., $\Delta=0$). For all considered values of the small-scale parameter and slenderness ratio, Table 1 shows that there is a reasonably good agreement between the predicted results by the RKPM and those of the AMM for both of the NTBT and NHOBT. In most of the cases, the RKPM could capture the predicted results by the AMM with relative error lower than 0.1 percent.

In another comparison study, the predicted frequencies of a system of doubly parallel nanotubes based on the suggested models are verified with those of existing data in the literature. In Ref. [39], free transverse vibration of double-nanobeam systems with simple ends was examined by using nonlocal Euler–Bernoulli beam theory (NEBT). In-phase and out-of-phase modes were identified and their corresponding natural frequencies were evaluated analytically. According to Ref. [39], the constitutive simply supported tubes do not have any mislocation and their properties are as follows: $E_{b_1}=E_{b_2}=0.971$ TPa, $r_{m_1}=r_{m_2}=0.34$ nm,

t_b=0.34 nm, $\rho_{b_1}=\rho_{b_2}$ = 2300 kg/m^3, and l_b=20 nm. The vdW forces between these identical tubes were considered by a uniform vdW density function of magnitude $C_{vdW}=\overline{C}_{vdW}E_{b_1}I_{b_1}/l_{b_1}^5$ where $\overline{C}_{vdW}$ = 10. The predicted dimensionless fundamental frequency of the nanosystem (i.e., $\varpi_1=\omega_1 l_{b_1}^2\sqrt{\rho_{b_1}A_{b_1}/E_{b_1}I_{b_1}}$ where ω_1 is the fundamental frequency) by the suggested models and that of Ref. [39] as a function of the dimensionless small-scale parameter have been demonstrated in Fig. 2. According to the plotted results, there is a fairly good agreement between the obtained results by the proposed models and those of Ref. [39]. Additionally, the predicted frequencies by the proposed models are somewhat lower than those of Ref. [39]. It is mainly related to the incorporation of both rotary inertia and shear deformation effects into the deformation fields of the nanosystem modeled based on the NTBT or the NHOBT.

6.2. Numerical studies

In this part, the roles of the aspect ratio, intertube free space, mislocation, small-scale parameter, slenderness ratio, radius of the nanotubes, transverse and rotational stiffness of the surrounding elastic medium on free vibration behavior of the nanosystem are aimed to be examined. In all demonstrated results, the dotted-dashed and the solid lines in order are associated with the NTBT and the NHOBT.

6.2.1. Influence of the aspect ratio

The effect of the length of one tube to that of another, called aspect ratio of the nanosystem, on free vibration of DPSWCNTs is of particular interest. In Fig. 3(a)–(c), the predicted first five natural frequencies of the nanosystem in terms of the aspect ratio are provided for SS, CC, and CF boundary conditions. The length of the first nanotube has been kept fixed, λ_1=30, $(e_0a)_1$ = 2 nm, Δ = 0, and the interactions of the nanotubes with their surrounding medium have been ignored. For all given end conditions, both NTBT and NHOBT predict that the first two natural frequencies would commonly reduce by an increase of the aspect ratio. These results are explained by this fact that the transverse stiffness of the nanosystem would commonly reduce as the aspect ratio increases. However, the third frequency of the nanosystem increases with the aspect ratio up to a certain level. For aspect ratios greater than this level, the third frequency decreases by an increase of the aspect ratio. No regular pattern is observed for the fourth and fifth frequencies in terms of the aspect ratio; however, the general trend of the demonstrated results is descending. As it is seen in Fig. 3(a)–(c), such a reduction is more obvious for lower levels of aspect ratio. For all considered end conditions, variation of the aspect ratio is more influential on the change of the fundamental frequency with respect to other ones. A detailed survey of the plotted results reveals that the discrepancies between the results of the NTBT and those of the NHOBT generally increase with the mode number. Irrespective of the considered boundary condition, the discrepancies between the predicted fundamental frequencies by the NTBT and those of the NHOBT would commonly decrease as the aspect ratio increases.

6.2.2. Influence of the intertube free space

An important study has been performed to investigate the role of the intertube free space on the vibration behavior of the nanosystem under different end conditions. In Fig. 4(a)–(c), the plots of the fundamental frequency of the nanosystem as a function of free space ratio, defined by $d_0/t_b=d-(r_{m_1}+r_{m_2}+t_b)/t_b$, are provided for three levels of the small-scale parameter (i.e., e_0a = 0, 1, and 2 nm) and three boundary conditions. The SWCNTs are prohibited from any interaction with the surrounding medium (i.e., $K_t=K_r$=0), and λ_1=20. Generally, by an increase of the free space, the fundamental frequency of the nanosystem decreases. Such a fact is more (less) obvious for nanosystems with CF (CC) boundary condition. This fact is mainly related to the flexural stiffness of the nanostructure. As the nanosystem becomes stiffer, the effect of the vdW interaction force on its deflection becomes lesser. In other words, the ratio of the vdW elastic energy to the elastic strain energy of the nanosystem would reduce by increasing of the free space. As the intertube free space goes beyond a particular level, each tube would vibrate independently from its neighboring tube

Table 1
The predicted first five natural frequencies of doubly parallel SWCNTs based on the NTBT and NHOBT via RKPM and AMM for several values of the small-scale parameter and slenderness ratio ($K_t=K_r$=0, Δ = 0).

λ_1	e_0a = 0 nm				e_0a = 1 nm				e_0a = 2 nm			
	NTBT		NHOBT		NTBT		NHOBT		NTBT		NHOBT	
	RKPM	AMM	RKPM	AMM	RKPM	AMM	RKPM	AMM	RKPM	AMM	RKPM	AMM
10	1.55760	1.55743	1.64620	1.64485	1.49426	1.49408	1.57924	1.57795	1.34242	1.34223	1.41875	1.41757
	1.83017	1.83003	1.90325	1.90208	1.77663	1.77642	1.84570	1.84452	1.65111	1.65072	1.71052	1.70932
	4.44797	4.44769	5.00508	5.00076	3.83335	3.83304	4.31329	4.30967	2.88004	2.87966	3.24040	3.23769
	4.54894	4.54867	5.09152	5.08727	3.95015	3.94977	4.41337	4.40974	3.03389	3.03325	3.37254	3.36971
	7.48645	7.48599	8.77138	8.76256	5.61236	5.61187	6.57488	6.56878	3.69001	3.68935	4.32229	4.31832
15	0.76894	0.76878	0.79270	0.79199	0.75457	0.75440	0.77788	0.77718	0.71585	0.71567	0.73796	0.73728
	1.23758	1.23748	1.25105	1.25060	1.22874	1.22859	1.24175	1.24127	1.20546	1.20519	1.21725	1.21667
	2.47076	2.47054	2.67399	2.67178	2.30007	2.29984	2.48921	2.48717	1.94383	1.94356	2.10361	2.10187
	2.64919	2.64898	2.83611	2.83402	2.49082	2.49053	2.66267	2.66068	2.16631	2.16582	2.30636	2.30454
	4.44804	4.44770	5.00522	5.00077	3.83341	3.83305	4.31340	4.30968	2.88009	2.87967	3.24048	3.23770
30	0.20816	0.20801	0.21012	0.20983	0.20717	0.20702	0.20912	0.20883	0.20428	0.20413	0.20620	0.20591
	0.76895	0.76878	0.79272	0.79199	0.75458	0.75440	0.77790	0.77718	0.71586	0.71567	0.73797	0.73728
	1.00592	1.00589	1.00617	1.00611	1.00573	1.00568	1.00598	1.00590	1.00517	1.00509	1.00541	1.00530
	1.24080	1.24069	1.25422	1.25376	1.23198	1.23183	1.24495	1.24446	1.20875	1.20848	1.22050	1.21993
	1.55766	1.55743	1.64628	1.64486	1.49432	1.49408	1.57932	1.57795	1.34248	1.34223	1.41882	1.41757
60	0.05331	0.05322	0.05347	0.05335	0.05325	0.05316	0.05340	0.05328	0.05306	0.05297	0.05321	0.05309
	0.20805	0.20795	0.21001	0.20977	0.20706	0.20696	0.20901	0.20877	0.20416	0.20407	0.20609	0.20585
	0.45199	0.45187	0.46064	0.46020	0.44718	0.44706	0.45574	0.45530	0.43362	0.43350	0.44192	0.44148
	0.76888	0.76872	0.79266	0.79193	0.75450	0.75434	0.77784	0.77711	0.71577	0.71560	0.73791	0.73721
	1.11445	1.11445	1.11446	1.11445	1.10939	1.10915	1.11445	1.11445	1.02557	1.02533	1.07047	1.06945

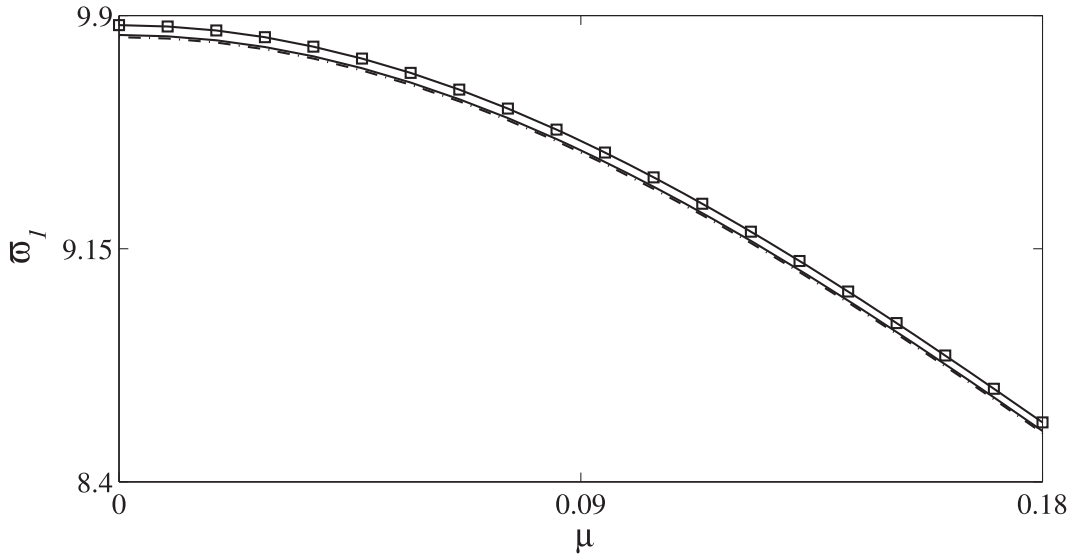

Fig. 2. Comparison of the predicted fundamental frequency of a double-nanobeam system by the proposed models and that based on the model of Murmu and Adhikari [39]: ((– –) NTBT, (—) NHOBT, (□) Ref. [39]; $\bar{C}_{vdW} = 10$, $K_r = K_t = 0$, $\Delta = 0$).

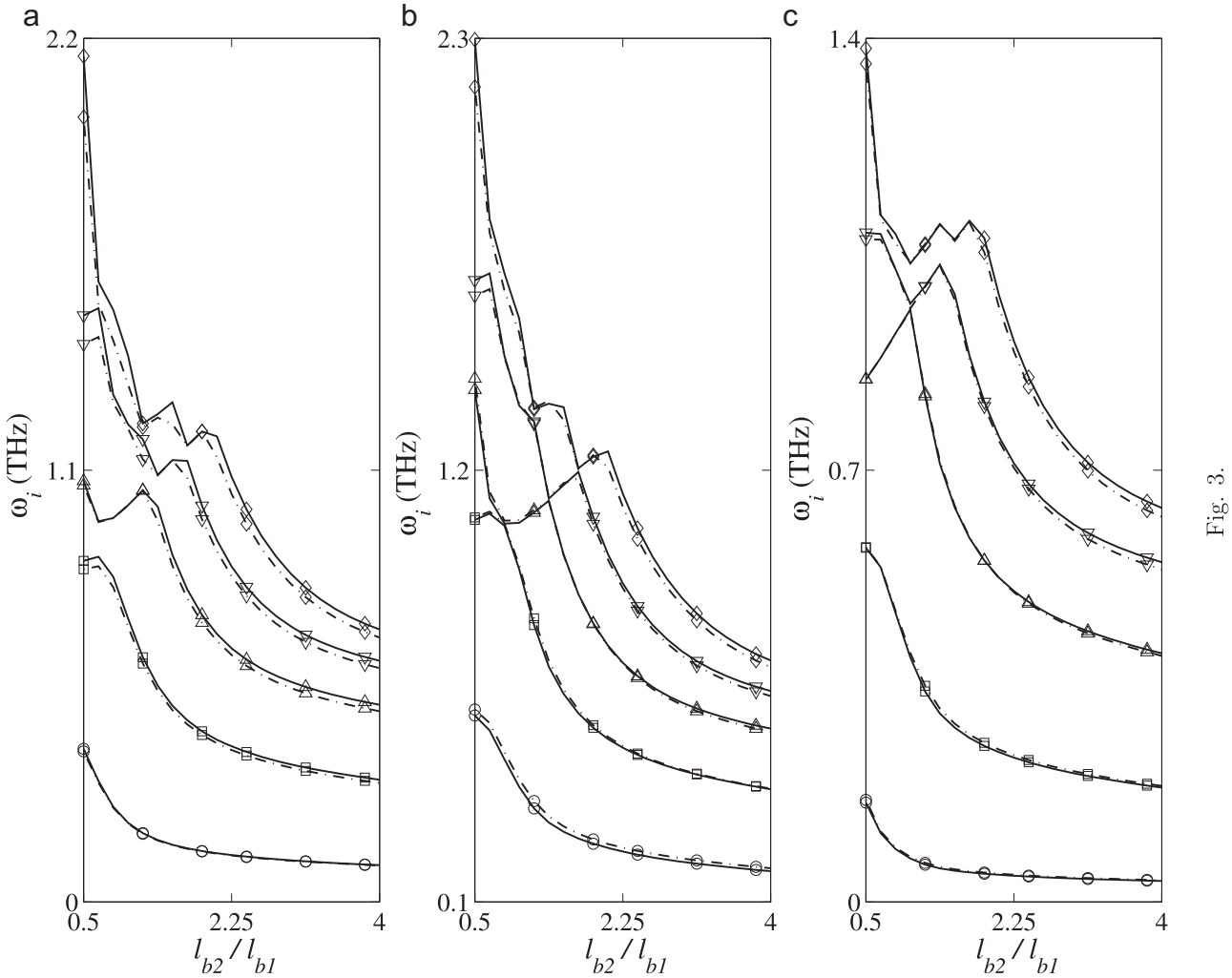

Fig. 3. Effect of the aspect ratio of the constitutive SWCNTs of the nanosystem on its first five frequencies for various boundary conditions: (a) SS, (b) CC, and (c) CF ((○) ω_1, (□) ω_2, (△) ω_3, (▽) ω_4, (◇) ω_5; $\lambda_1 = 30$, $e_0a = 2$ nm).

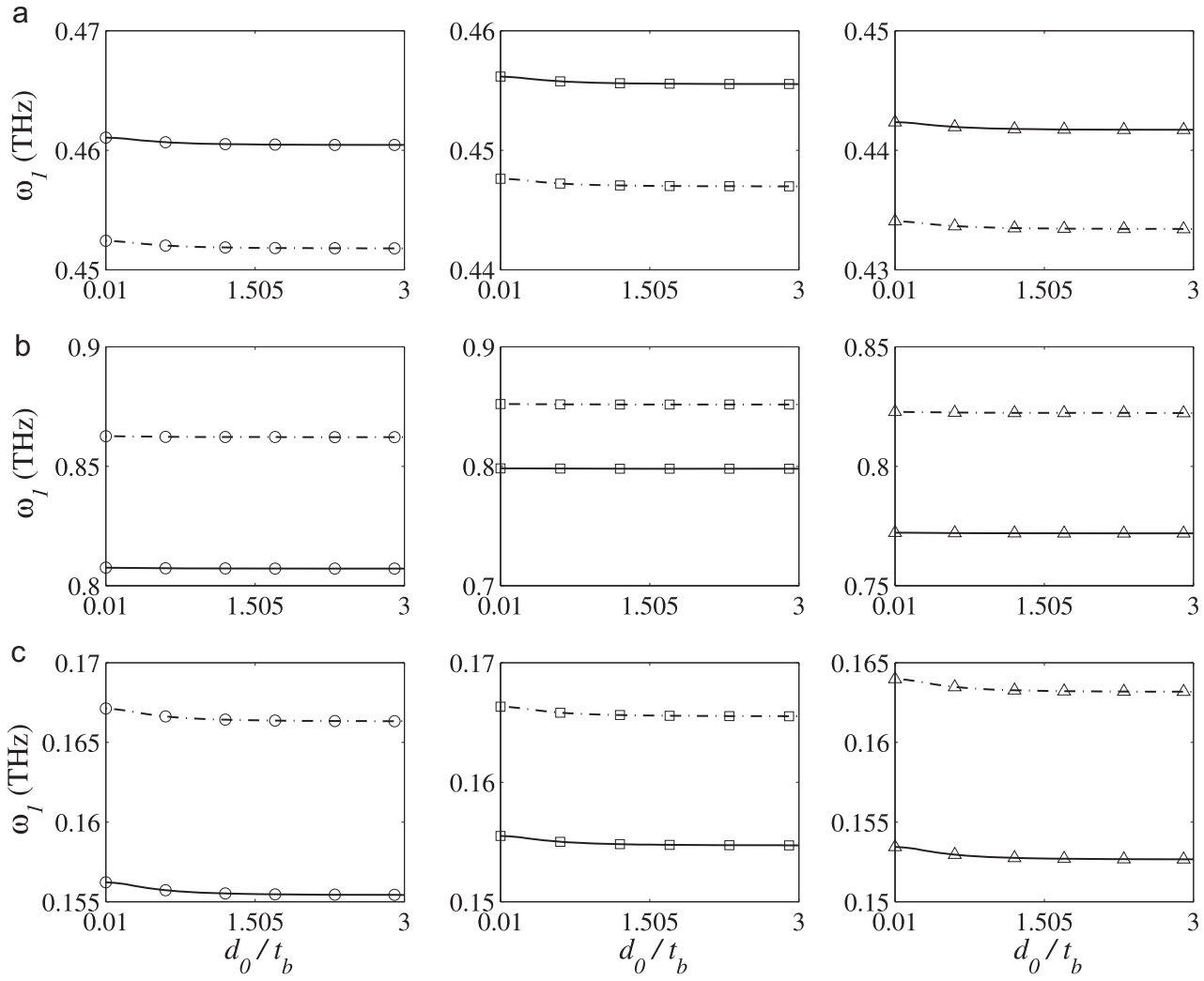

Fig. 4. Effect of the intertube free space on the fundamental frequency of the nanosystem for various boundary conditions: (a) SS, (b) CC, and (c) CF ((○) $e_0a = 0$, (□) $e_0a = 1$, (△) $e_0a = 2$ nm; $\lambda_1 = 20$).

since the influence of the intertube vdW forces becomes negligible. A more detailed survey of the obtained results shows that the NTBT could reproduce the results of the NHOBT for SS, CC, and CF conditions with relative error lower than 1.9, 6.8, and 7 percent, respectively. In the case of the nanosystem with SS boundary condition, by an increase of the free space, the discrepancies between the predicted fundamental frequencies by the NTBT and those of the NHOBT would slightly increase. However, in the cases of the CC and CF boundary conditions, such discrepancies would trivially decrease by increasing of the free space.

The influence of the intertube free space on higher frequencies of the nanosystem is also of interest. To this end, the plots of the first five frequencies of the nanosystem as a function of free space ratio are demonstrated in Fig. 5(a)–(c). Such results are given for different boundary conditions in the case of $e_0a = 2$ nm. As it is seen in these figures, both NTBT and NHOBT predict that the second and fourth frequencies of the nanosystem gradually reduce as the intertube free space magnifies. Irrespective of the boundary conditions of the nanosystem, such a reduction is more obvious for lower levels of the intertube free space. However, the third and fifth frequencies sharply decrease as the free space increases up to a certain value. For free spaces greater than such a certain value, variation of the free space has a trivial influence on the variation of third and fifth frequencies. A more detailed study of the plotted results reveals that there does not exist a direct relationship between the discrepancies of the results of the proposed models and the mode number. For instance, in the case of SS(CC) boundary condition, the NTBT could reproduce the predicted first five frequencies by the NHOBT sequentially with relative errors lower than 2(6.5), 5.5(6.5), 5.5(3), 5.5(7), and 8.5(5.5) percent for the considered range of the free space ratio. For all considered boundary conditions, the discrepancies between the predicted fundamental frequency by the NTBT and that of the NHOBT are trivially affected by the variation of the intertube free space. However, for higher frequencies, such discrepancies would grow as the free space ratio increases.

6.2.3. *Influence of the mislocation*

The doubly parallel SWCNTs of equal lengths may be placed not exactly in front of each other. In such a situation, the coordinates of the end points of the constitutive tubes are dissimilar, which is called mislocation effect. This part is devoted to recognize and understand the role of mislocation on vibrations of elastically embedded DPSWCNTs. For this purpose, the plotted results of the first five natural frequencies of the nanosystem in terms of mislocation ratio (i.e., Δ/l_{b_1}) have been provided in Fig. 6(a)–(c) for various end conditions. These plots have been demonstrated for a nanosystem that consists of two identical SWCNTs whose

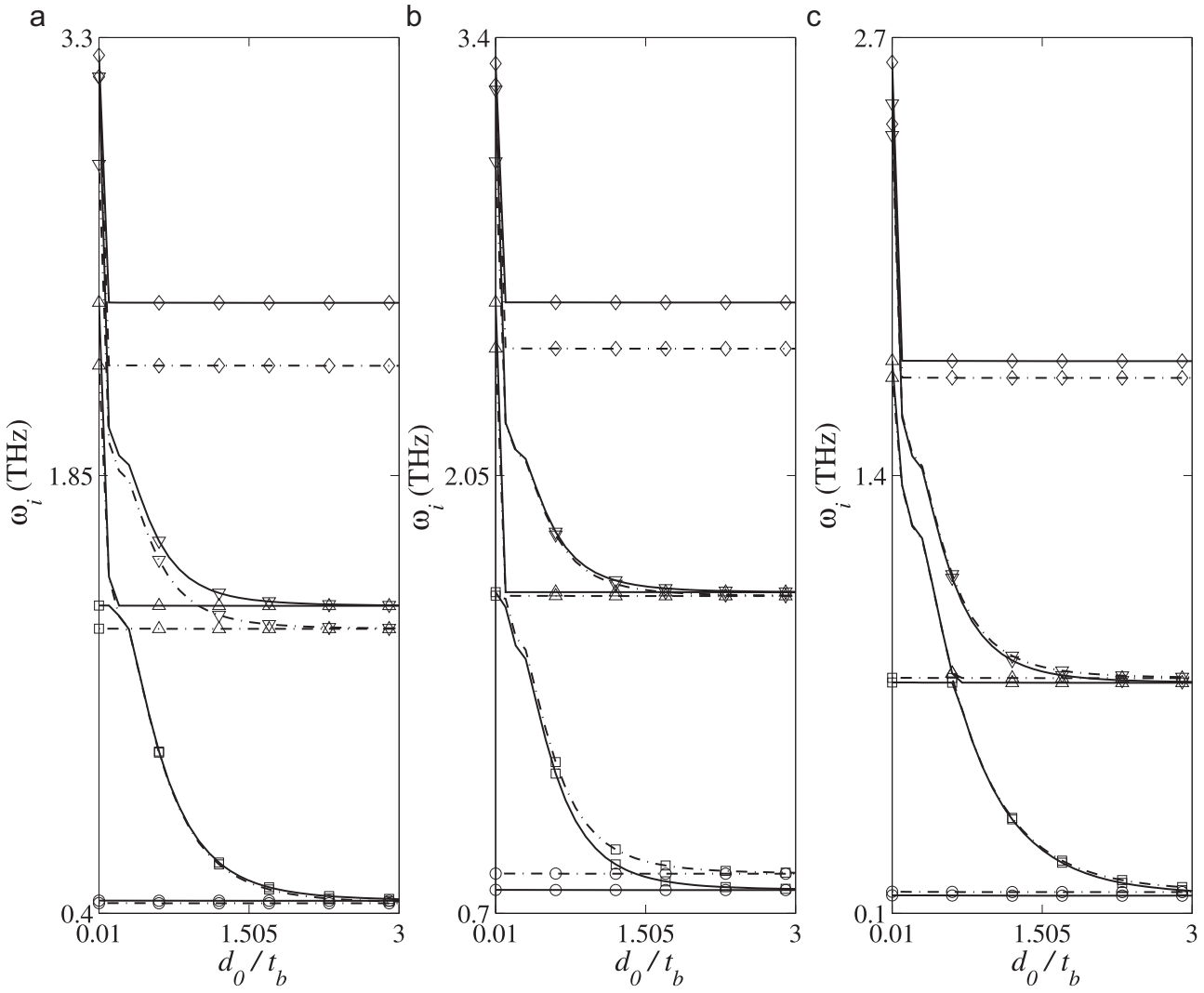

Fig. 5. Effect of the intertube free space on the first five frequencies of the nanosystem for various boundary conditions: (a) SS, (b) CC, and (c) CF ((○) ω_1, (□) ω_2, (△) ω_3, (▽) ω_4, (◇) ω_5; $\lambda_1=20$, e_0a = 2 nm).

slenderness ratio and small-scale parameter are equal to 20 and 2 nm, respectively. According to the demonstrated results, irrespective of the considered end conditions, the plots of the fundamental frequency as a function of mislocation ratio consist of two branches: an ascending branch and a descending one. Such plots take their absolute maximum points at special points. For example, in the cases of SS, CC, and CF boundary conditions, the maximum fundamental frequency of the nanosystem in order takes place at the mislocations about $0.43l_{b_1}$, $0.4l_{b_1}$, and $0.36l_{b_1}$. Among understudy nanosystems, mislocation has the most(less) influence on the fundamental frequency of DPSWCNTs with SS(CF) ends. Regarding the capability of the NTBT in capturing the results of the NHOBT, a close survey indicates that the NTBT could reproduce the predicted fundamental frequency by the NHOBT for SS, CC, and CF boundary conditions with relative error lower than 2, 8.5, and 7.3 percent, respectively. Additionally, the maximum discrepancies between the predicted fundamental frequency by the NTBT and that of the NHOBT generally occur at the points near to the above-mentioned special mislocations. Concerning the second vibration mode of the mislocated DPSWCNTs, its frequency commonly decreases with the mislocation until its value approaches to the fundamental frequency at a mislocation approximately equal to the length of the nanotube. For nanosystems with SS and CC end conditions, the discrepancies between the predicted second frequency by the NTBT and that by the NHOBT commonly magnify as the mislocation increases. In the case of the CF boundary condition, no regular pattern for the variation of such a discrepancy as a function of the mislocation is observed. In the case study at hand, for the considered range of the mislocation ratio, the NTBT could capture the second frequency of the NHOBT for SS, CC, and SC conditions with relative error lower than 2, 6.5, and 5.7 percent, respectively. Concerning the role of mislocation on the third, fourth, and fifth natural frequencies of the nanosystem, no regular patterns for the plots of these frequencies in terms of mislocation are detected. Generally, for higher modes of vibrations, greater discrepancies between the results of the NTBT and those of the NHOBT are observed.

6.2.4. *Influence of the small-scale parameter*

The nonlocality plays an important role in vibrations of nanostructures. In this part, the effect of the small-scale parameter on the free vibration of elastically embedded DPSWCNTs is aimed to be understood. To this end, the predicted fundamental frequency of the nanosystem based on the NTBT and NHOBT as a function of the small-scale parameter for various end conditions is plotted in Fig. 7(a)–(c). The provided results are related to

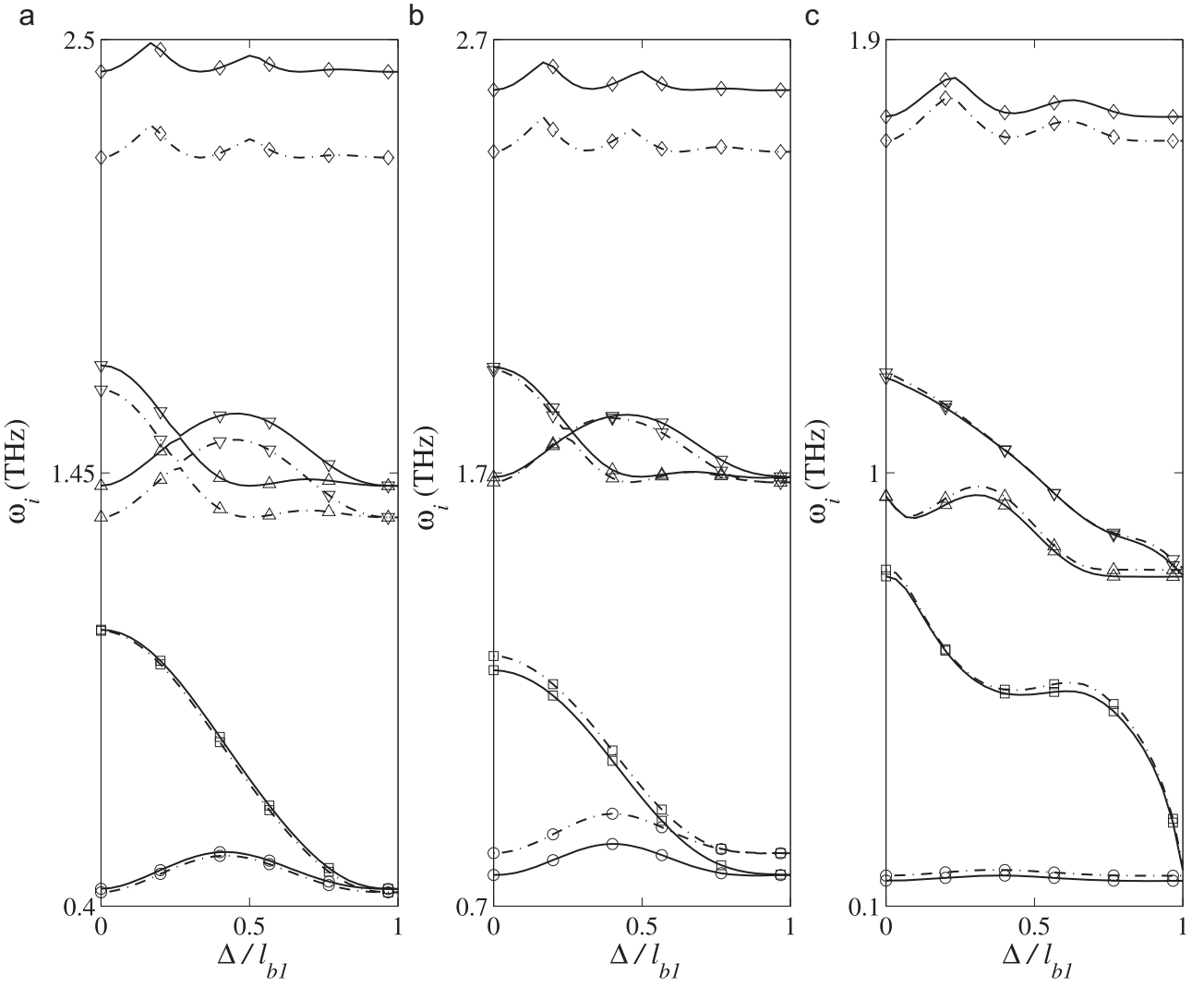

Fig. 6. Effect of the mislocation of the constitutive SWCNTs of the nanosystem on its first five frequencies for various boundary conditions: (a) SS, (b) CC, and (c) CF ((○) ω_1, (□) ω_2, (△) ω_3, (▽) ω_4, (⋄) ω_5; $\lambda_1=20$, e_0a = 2 nm).

nanosystems with similar nanotubes whose slenderness ratios are 10, 15, and 30. The proposed models based on the NTBT and NHOBT predict that the fundamental frequency of the nanosystem generally reduces as the small-scale parameter increases. For a given small-scale parameter, by an increase of the slenderness ratio of the constitutive tubes of the nanosystem, its fundamental frequency would lessen. Additionally, variation of the small-scale parameter has more influence on the fundamental frequencies of stockier nanosystems, irrespective of its boundary conditions. Among the considered boundary conditions, variation of the small-scale parameter has the most(less) effect on the variation of the fundamental frequency of nanosystems with CC(CF) end conditions. Regarding the capability of the NTBT in capturing the fundamental frequency of the nanosystem based on the NHOBT, the NTBT can produce the results of the NHOBT for SS, CC, and CF end conditions and $\lambda_1=(10,15,30)$ with relative error lower than (5.5,3,0.1), (6.1,7.4,4.9), and (16.5,10.5,3.8), respectively. In the case of the nanosystem with SS end conditions, variation of the small-scale parameter has a trivial effect on the discrepancies between the obtained results by the NTBT and those of the NHOBT. However, in the cases of the CC and CF end conditions, such discrepancies decrease to some extent as the small-scale parameter grows.

We are also interested in the role of the small-scale parameter on the natural frequencies pertinent to higher vibration modes. In Fig. 8(a)–(c), the plots of the first five natural frequencies of the nanosystem with $\lambda_1=30$ in terms of the small-scale parameter have been demonstrated for various end conditions. These figures display that all natural frequencies reduce as the small-scale parameter increases. Generally, the rate of reduction for frequencies associated with higher modes is more apparent. The discrepancies between the results of the NTBT and those of the NHOBT are fairly more obvious for higher vibration modes. In the case of SS condition, for all considered modes of vibration, such discrepancies do slightly alter as a function of the small-scale parameter. Further, the NTBT could capture the first, second, third, fourth, and fifth frequencies of the nanosystem analyzed by the NHOBT with relative error lower than 0.9, 3, 0.1, 1.1, and 5.5 percent, respectively. In the case of CC boundary condition, for the first four natural frequencies, these discrepancies would reduce as the small-scale parameter magnifies. However, concerning the fifth mode of vibration, such discrepancies would slightly grow as the small-scale parameter increases. In addition, the NTBT can produce the first to fifth frequencies by the NHOBT with a relative error lower that 4.9, 1.2, 0.75, 0.7, and 2.6 percent, sequentially. Concerning the nanosystem with CF end condition, the above-

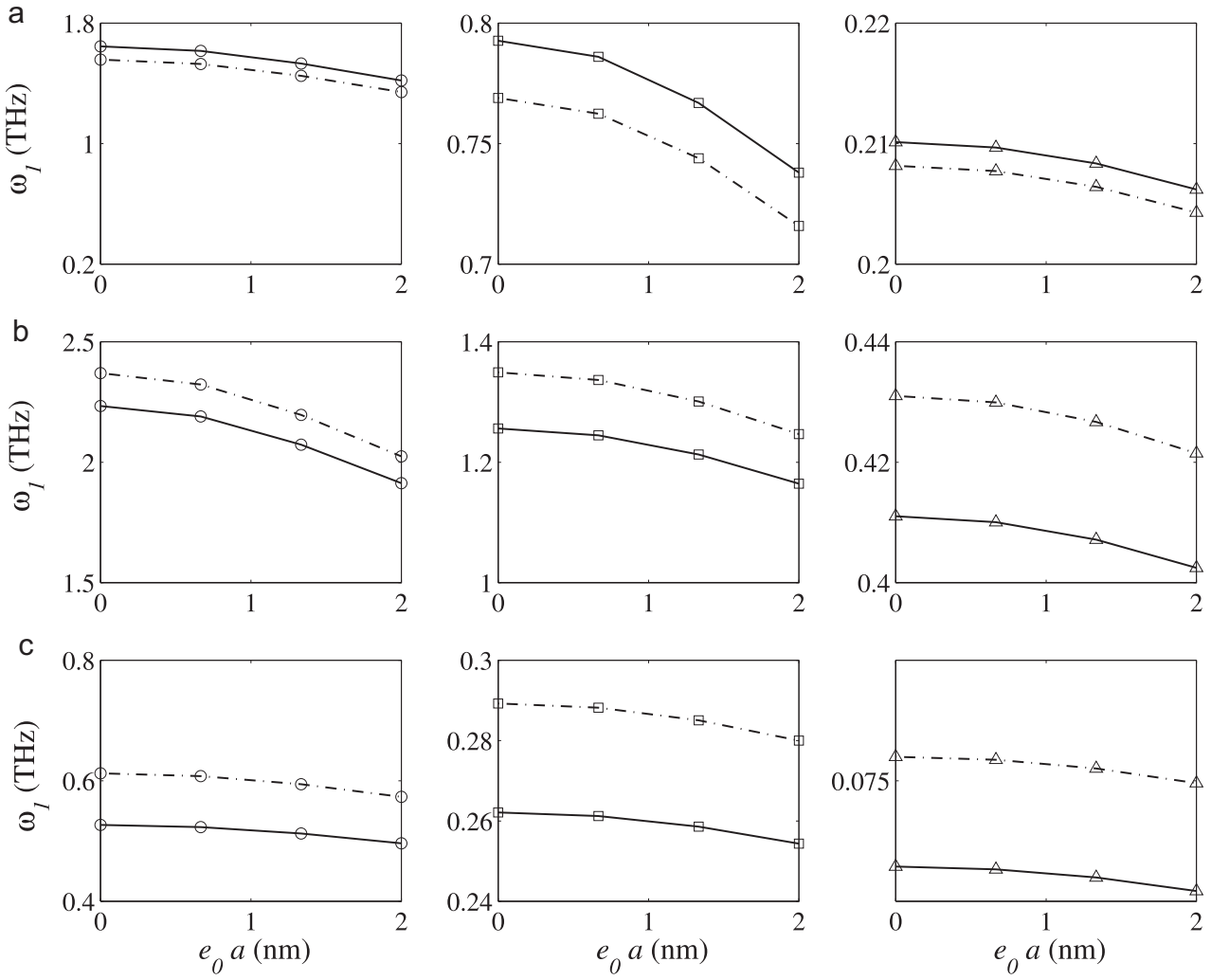

Fig. 7. Effect of the small-scale parameter on the fundamental frequency of the nanosystem for various boundary conditions: (a) SS, (b) CC, and (c) CF ((○) $\lambda_1=10$, (□) $\lambda_1=15$, (△) $\lambda_1=30$).

mentioned discrepancies of the first, second, and fifth frequencies would reduce as the small-scale parameter increases. However, these discrepancies for the frequencies associated with the third and fourth vibration modes would magnify with the small-scale parameter. Additionally, the NTBT could capture the first, second, third, fourth, and fifth frequencies of the nanosystem on the basis of the NHOBT with relative error lower than 3.8, 1.8, 0.1, 1.1, and 1 percent, respectively.

6.2.5. Influence of the slenderness ratio

The slenderness ratio is one of the most important geometry characteristics of nanotube structures that significantly affects their flexural and shear dynamic displacements. Therefore, its influence on the dynamics of elastically embedded DPSWCNTs is also of great importance and should be investigated. In Fig. 9(a)–(c), the first five frequencies of the nanosystem with $e_0a = 2$ nm in terms of the slenderness ratio have been demonstrated for various boundary conditions. Concerning the first two natural frequencies of the nanosystem, such frequencies decrease as the slenderness ratio increases. Additionally, the discrepancies between the results of the NTBT and those of the NHOBT would decrease with the slenderness ratio. In the cases of the SS, CC, and CF end conditions, the NTBT in order could capture the fundamental(second) frequency of the nanosystem with relative error lower than 2(4), 6.5 (2.7), and 6.9(1.8) for the considered range of the slenderness ratio. Regarding the third, fourth, and fifth frequencies of the nanosystem, these frequencies commonly reduce as the slenderness ratio increases. However, in some intervals of the slenderness ratio, such frequencies would magnify in terms of the slenderness ratio. In the case of nanosystems with SS, CC, and CF boundary conditions, the NTBT could generate the (third, fourth, fifth) frequency of the NHOBT with relative error lower than (3.5, 5.5, 8.6), (0.7, 2, 5.5), and (1, 2.2, 2.9) percent, respectively. However, no regular patterns for the discrepancies between the results of the NTBT and those of the NHOBT as a function of the slenderness ratio are observed.

6.2.6. Influence of the radius of the SWCNTs

Another crucial study is performed to investigate the role of the radius of the SWCNTs on the vibration behavior of the elastically embedded nanosystem. Fig. 10(a)–(c) shows the plots of the first five frequencies of the nanosystem as a function of radius ratio (i.e., r_{m_1}/r_{m_0}) for different boundary conditions and three levels of the small-scale parameter (i.e., $e_0a = 0$, 1, and 2 nm). The nanosystem has identical tubes of length 20 nm in which their interactions with the surrounding elastic medium have been provoked and there exists no mislocation (i.e., $\Delta = 0$). Both NTBT and NHOBT predict that the fundamental frequency of the nanosystem magnifies as the mean radius of the constitutive SWCNTs of the nanosystem increases. This is chiefly related to this fact that not only

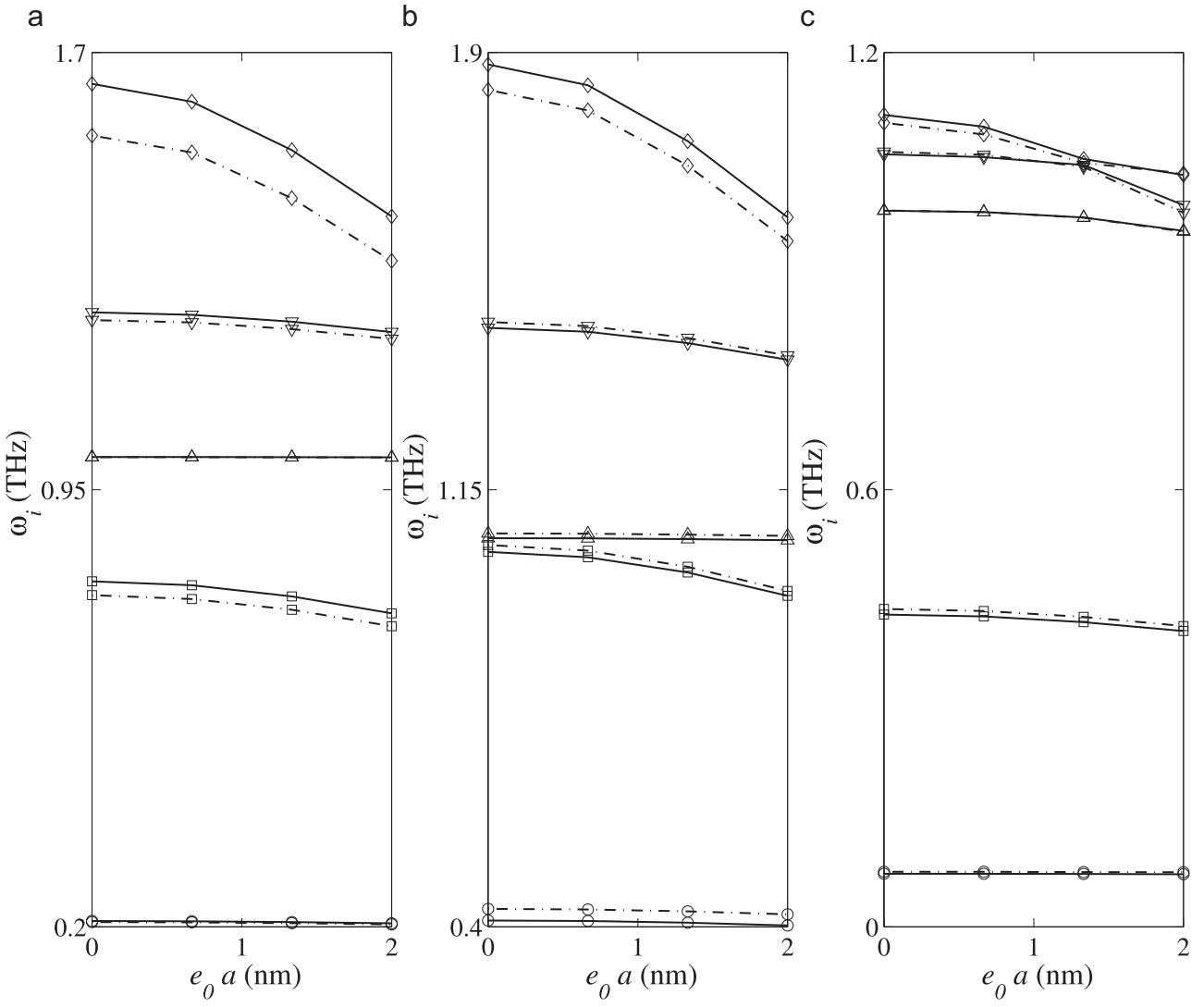

Fig. 8. Effect of the small-scale parameter on the first five frequencies of the nanosystem for various boundary conditions: (a) SS, (b) CC, and (c) CF ((○) ω_1, (□) ω_2, (△) ω_3, (▽) ω_4, (◇) ω_5; $\lambda_1=30$).

the flexural stiffness of the nanosystem, but also the intertube vdW interactional force magnifies as the radius of the tubes increases. The rising of these factors lead to an increase of the transverse stiffness of the nanosystem. In the cases of the SS and CF end conditions, the discrepancies between the predicted fundamental frequencies by the NTBT and those of the NHOBT would generally increase as the mean radius of the tubes grows. However, in the case of the CC end condition, such discrepancies would reduce with the mean radius up to a special level, thereafter, these discrepancies would again increase as the mean radius of the nanotubes magnifies. For the given range of the mean radius, the NTBT can produce the fundamental frequency of the NHOBT with relative error lower than 17.6, 9, and 31 percent for SS, CC, and CF boundary conditions, respectively. Generally, the above-mentioned discrepancies in the case of the CF end conditions are more obvious with respect to other cases. Concerning the second frequency, the proposed models predict that such a frequency commonly increases as the mean radius of the nanotubes increases. Further studies also explain that the discrepancies between the predicted second frequencies by the NTBT and those of the NHOBT are generally lower than those obtained for the first mode of vibration of the nanosystem. For instance, the NTBT could produce the second frequencies of the nanosystem based on the NHOBT with relative error lower than 16, 8, and 18.5 percent in the cases of the SS, CC, and CF boundary conditions, respectively. Regarding the third, fourth and fifth frequencies of the nanosystem, no regular variations of these frequencies in terms of the mean radius of the nanotubes are detectable. However, the discrepancies between these frequencies based on the NTBT and those of the NHOBT would generally increase as the radius of the constitutive tubes magnifies.

6.2.7. Influence of the transverse stiffness of the surrounding medium

In the previous parts, the effect of the surrounding elastic medium on free vibration behavior of the nanosystem had been ignored since the influence of the considered parameter on the free dynamic response of the nanostructure was particularly of concern. In the present and upcoming parts, the confinement effect of the elastic matrix on the fundamental frequency is going to be examined. In Fig. 11(a)–(c), the plots of the fundamental frequency of the elastically embedded nanosystem as a function of the dimensionless transverse stiffness of the surrounding medium (i.e., $\overline{K}_t = K_t I_{b_1}^4/E_{b_1} I_{b_1}$) are provided. The results have been presented for three boundary conditions as well as three levels of the slenderness ratio (i.e., $\lambda_1=15$, 20, and 25). According to the plotted

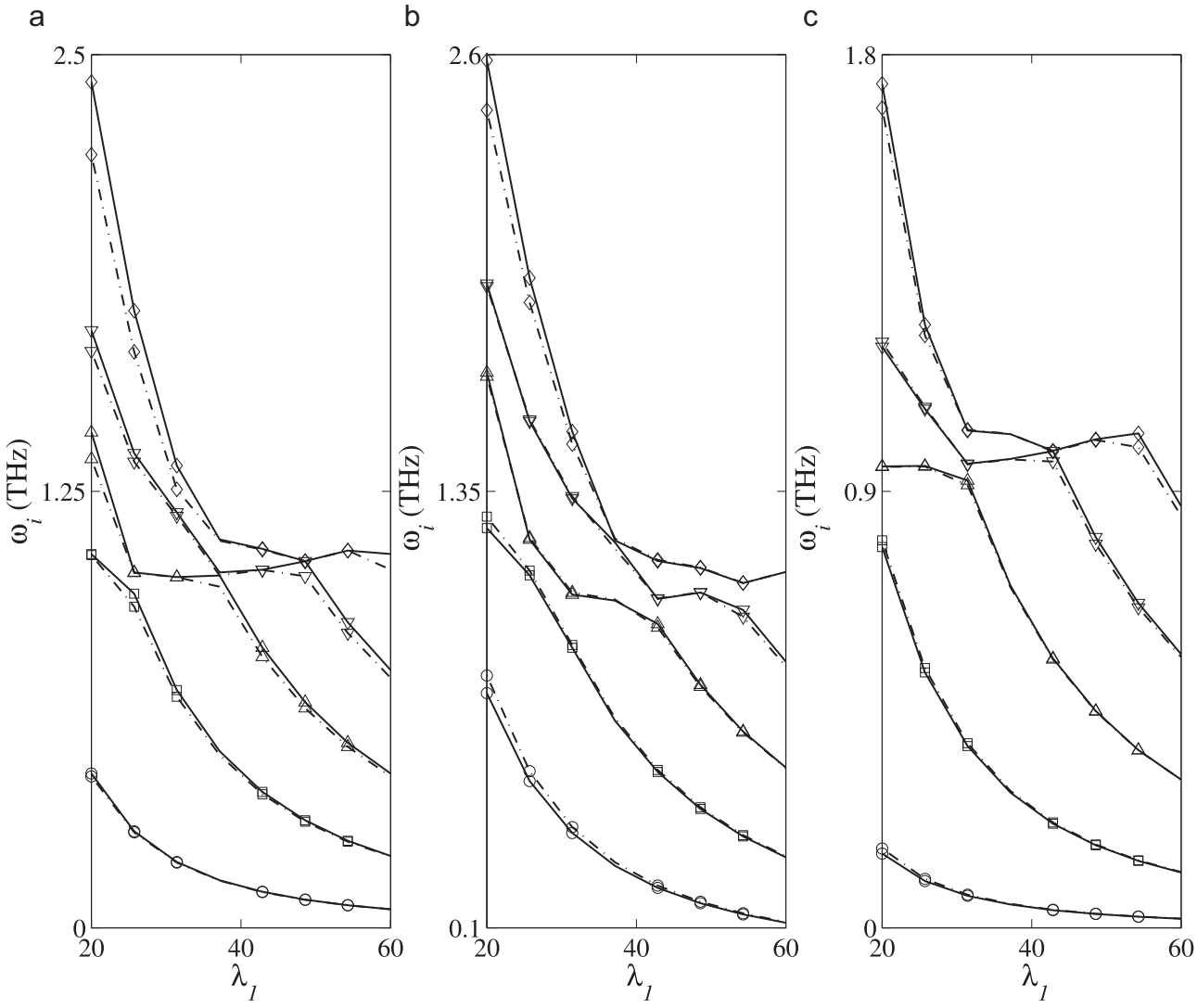

Fig. 9. Effect of the slenderness ratio of the constitutive SWCNTs of the nanosystem on its fundamental frequency for various boundary conditions: (a) SS, (b) CC, and (c) CF ((○) ω_1, (□) ω_2, (△) ω_3, (▽) ω_4, (⋄) ω_5; e_0a = 2 nm).

results, the fundamental frequency magnifies as the transverse stiffness of the surrounding medium increases. Such a fact holds true for all considered boundary conditions. Additionally, variation of the transverse stiffness has the most(less) influence on the variation of the fundamental frequency of the nanosystem with CF (CC) ends. As the slenderness ratio increases, the effect of the transverse stiffness of the surrounding medium on the fundamental frequency would lessen. For the considered boundary conditions, the discrepancies between the results of the NTBT and those of the NHOBT would reduce as the transverse stiffness magnifies. This is chiefly related to this fact that the share of the shear strain energy in the total elastic energy of the nanosystem decreases. It implies that the contribution of the shear displacement in the total displacement would reduce as the transverse stiffness of the elastic matrix increases. In the cases of SS, CC, and CF end conditions, the NTBT could capture the predicted results by the NHOBT for the slenderness ratio (15, 20, 25) with relative error lower than (3, 1.9, 0.13), (7.4, 6.8, 5.8), and (10, 7, 5) percent, respectively. Further studies have been performed to determine the role of the transverse stiffness on the frequencies of higher modes of vibration in which their figures have not been presented for the sake of conciseness. Such explorations show that the variation of the stiffness has the most influence on the variation of the fundamental frequency with respect to other ones.

6.2.8. Influence of the rotational stiffness of the surrounding medium

Consider the case that the rotation of each cross-section of the constitutive tubes of the nanosystem is not freely allowed due to the existence of high bonding between the nanotubes and their surrounding medium. Effect of such interactions on the free transverse vibration of the nanosystem is of our particular interest. To this end, the graphs of fundamental frequency of the elastically embedded DPSWCNTs in terms of the dimensionless rotational stiffness of the surrounding environment (i.e., $\overline{K}_r = K_r l_{b_1}^2/E_{b_1}I_{b_1}$) have been depicted in Fig. 12(a)–(c). The constitutive nanotubes are identical with e_0a = 1 nm and three levels of the slenderness ratio (i.e., λ_1 = 15, 20, and 25). The transverse interactions of nanotubes with their surrounding medium have been ignored to precisely address the role of only the rotational stiffness. According to the plotted results in Fig. 12(a)–(c), irrespective of the considered boundary condition, the fundamental frequency magnifies as the rotational stiffness of the surrounding medium increases. Such a fact is more obvious in the case of CF boundary conditions. However, fundamental frequency of the nanosystem with CC end conditions is less affected by the rotational stiffness. This fact is

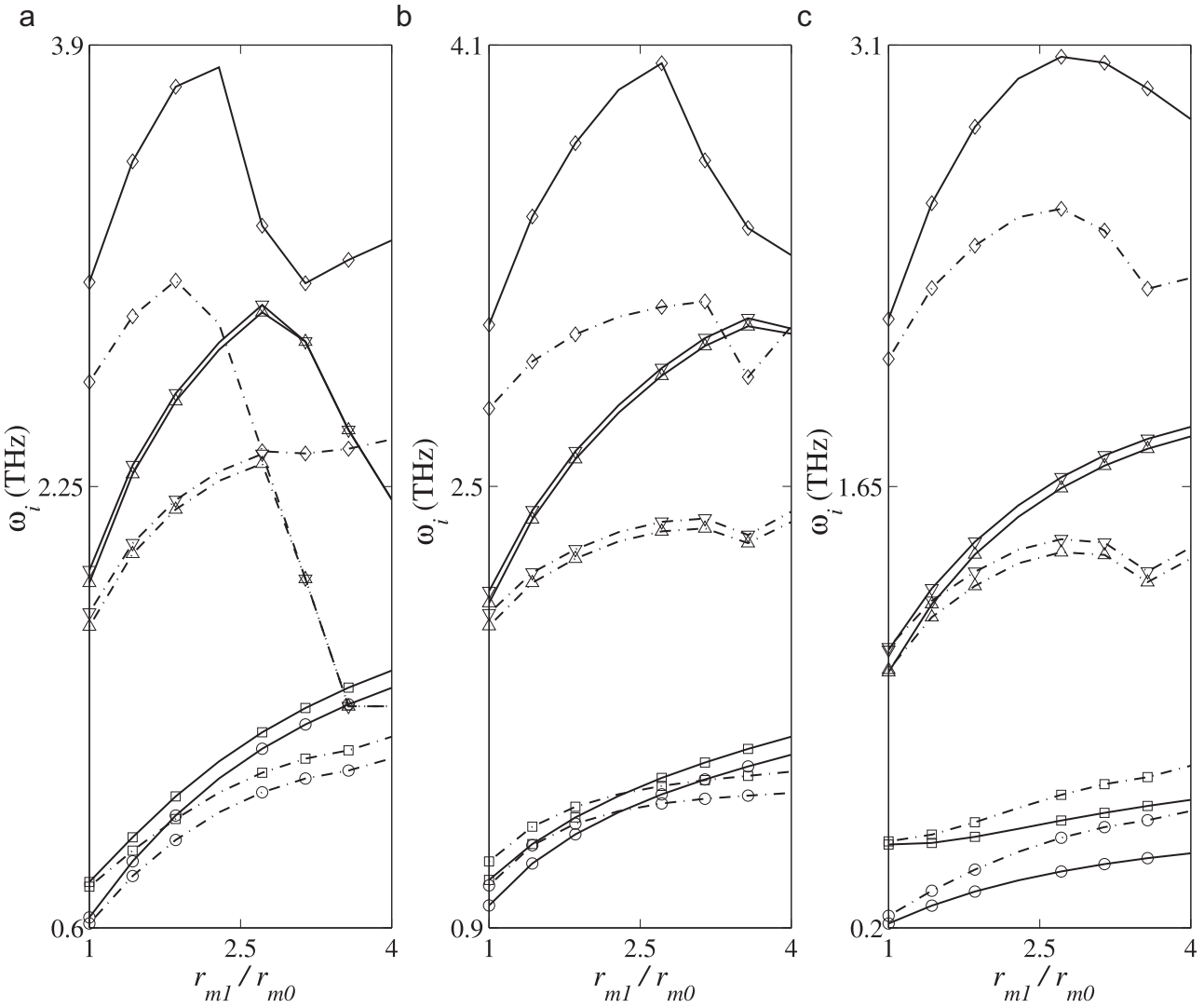

Fig. 10. Effect of the radius of the constitutive SWCNTs of the nanosystem on its five frequencies for various boundary conditions: (a) SS, (b) CC, and (c) CF ((○) ω_1, (□) ω_2, (△) ω_3, (▽) ω_4, (⋄) ω_5; $l_{b_1} = l_{b_2} = 20$ nm, $r_{m_0} = 2$ nm, $e_0a = 2$ nm).

related to the high ratio of the internal elastic energy of the nanosystem to that resulted from its rotational interaction with the surrounding elastic matrix. As the slenderness ratio of the nanosystem becomes lesser, the role of the rotational stiffness of the surrounding medium on the free vibration behavior of the nanosystem becomes more significant. It is mainly because of this fact that the ratio of the elastic energy resulted from rotational interaction of the nanotubes with the elastic matrix to that of the flexural and shear stiffness commonly grows as the slenderness ratio of the constitutive tubes of the nanosystem increases. A close scrutiny of the demonstrated results also reveals that the discrepancies between the results of the NTBT and those of the NHOBT would generally reduce as the rotational stiffness increases. Such a fact holds true for all considered end conditions. For a given rotational stiffness of the surrounding medium, the above-mentioned discrepancies would commonly lessen as the slenderness ratio magnifies. For the sake of brevity, the plots of frequencies of higher vibration modes have not been demonstrated. Further studies display that all natural frequencies of the elastically embedded nanosystem grow as the rotational stiffness increases. Additionally, for all vibration modes and all considered boundary conditions, the discrepancies between the results of the NTBT and those of the NHOBT would reduce as the rotational stiffness increases.

7. Conclusions

The free transverse vibrations of elastically embedded DPSWCNTs with arbitrary configuration are investigated in the context of the nonlocal continuum theory of Eringen. Using a new model for vdW interactional forces, Hamilton's principle is employed and the strong form of equations of motion is obtained based on the NTBT and NHOBT. A meshless technique is adopted to discretize the unknown fields of the proposed model and the nonlocal frequencies of the nanosystem are evaluated. A comprehensive parametric study is performed to address the roles of the influential factors, including radius and slenderness ratio of the constitutive tubes, intertube free space, mislocation, nonlocality, aspect ratio, and elastic properties of the surrounding medium, on the free dynamic response of the nanosystem. The capabilities of the NTBT in capturing the results of the NHOBT are noted through various numerical studies, and the discrepancies between their results are also determined and discussed. It is hoped that the obtained results have led to expand our views to the mechanism of dynamic interactions of doubly parallel tubes and its influential factors.

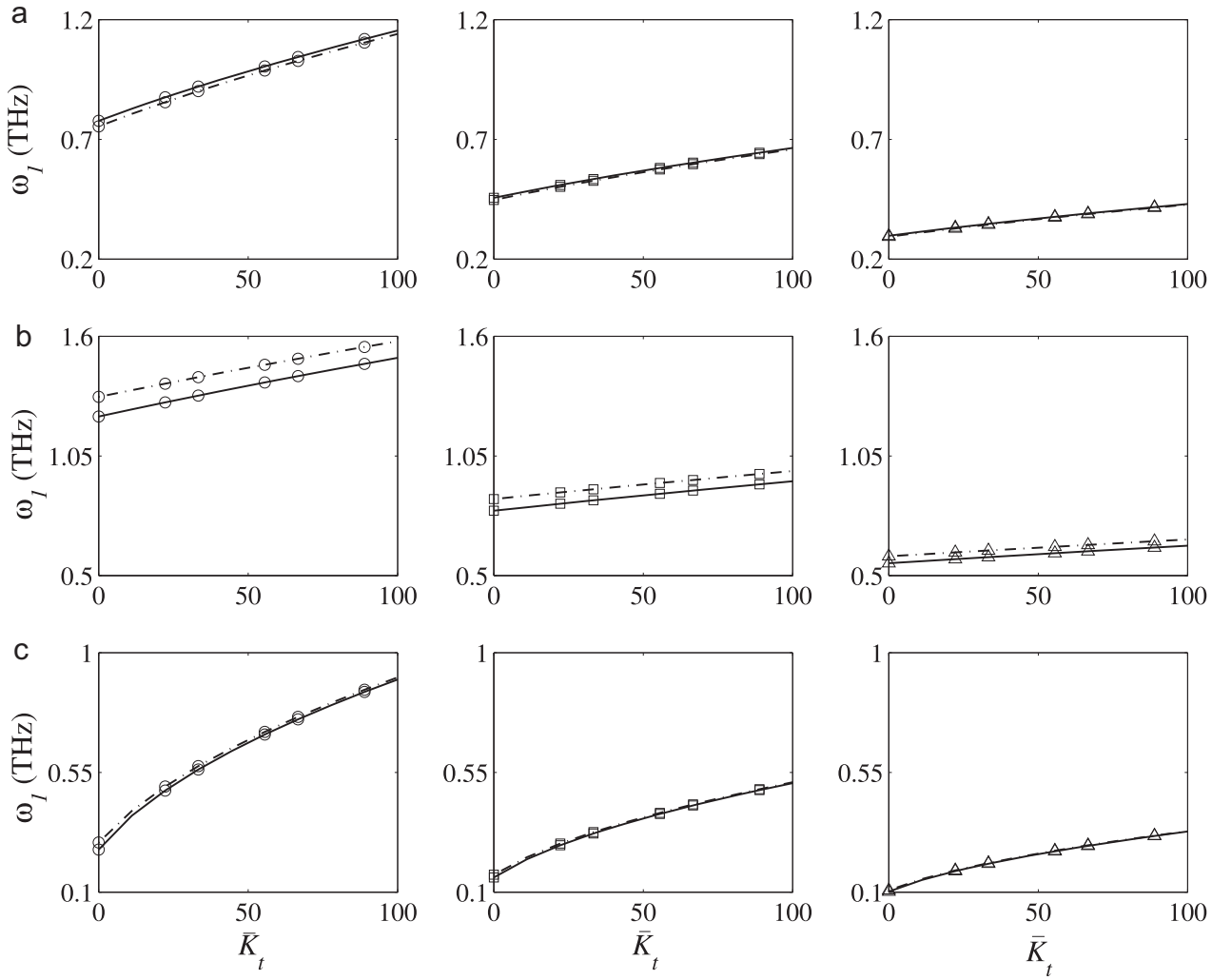

Fig. 11. Effect of the transverse stiffness of the elastic matrix on the fundamental frequency of the nanosystem for various boundary conditions: (a) SS, (b) CC, and (c) CF ((○) $\lambda_1=15$, (□) $\lambda_1=20$, (△) $\lambda_1=25$; $e_0a=1$ nm).

Acknowledgements

The financial support of Iran National Science Foundation (INSF) as well as Iran Nanotechnology Initiative Council is gratefully acknowledged. The author would also like to express his gratitude to the anonymous reviewers for their fruitful comments in which lead to the improvement of the present work.

Appendix A. Description of the mass and stiffness matrices of the proposed models using RKPM

A.1. The submatrices associated with the NTBT

$$\overline{\mathbf{w}}_i^T = < \overline{w}_{i_1}^T, \overline{w}_{i_2}^T, \ldots, \overline{w}_{i_{NP_i}}^T >^T ;\ i, j = 1, 2, \tag{A.1a}$$

$$\overline{\boldsymbol{\theta}}_i^T = < \overline{\theta}_{i_1}^T, \overline{\theta}_{i_2}^T, \ldots, \overline{\theta}_{i_{NP_i}}^T >^T , \tag{A.1b}$$

$$\left[\overline{\mathbf{M}}_b^T\right]_{IJ}^{w_iw_i} = \int_0^{\overline{r}_i} \varrho_1^{2i-2}\left(\phi_I^{w_i}\phi_J^{w_i} + \mu_i^{\,2}\phi_{I,\xi_i}^{w_i}\phi_{J,\xi_i}^{w_i}\right)\mathrm{d}\xi_i, \tag{A.1c}$$

$$\left[\overline{\mathbf{M}}_b^T\right]_{IJ}^{\theta_i\theta_i} = \int_0^{\overline{r}_i} \lambda_1^{-2}\varrho_2^{2i-2}\left(\phi_I^{\theta_i}\phi_J^{\theta_i} + \mu_i^{\,2}\phi_{I,\xi_i}^{\theta_i}\phi_{J,\xi_i}^{\theta_i}\right)\mathrm{d}\xi_i, \tag{A.1d}$$

$$\left[\overline{\mathbf{K}}_b^T\right]_{IJ}^{w_iw_i} = \int_0^{\overline{r}_i}\left(\begin{array}{l}\varrho_4^{2i-2}\phi_{I,\xi_i}^{w_i}\phi_{J,\xi_i}^{w_i} + \overline{K}_t^T\left(\phi_I^{w_i}\phi_J^{w_i} + \mu^2\phi_{I,\xi_i}^{w_i}\phi_{J,\xi_i}^{w_i}\right)+\\ \int_0^{\overline{\Lambda}_i}\overline{C}_{vdW}^T\left(\phi_I^{w_i} - \mu_i^{\,2}\phi_{I,\xi_i\xi_i}^{w_i}\right)\phi_J^{w_i}\mathrm{d}\xi_{3-i}\end{array}\right)\mathrm{d}\xi_i, \tag{A.1e}$$

$$\left[\overline{\mathbf{K}}_b^T\right]_{IJ}^{w_i\theta_i} = -\int_0^{\overline{r}_i}\varrho_4^{2i-2}\phi_{I,\xi_i}^{w_i}\phi_J^{\theta_i}\mathrm{d}\xi_i, \tag{A.1f}$$

$$\left[\overline{\mathbf{K}}_b^T\right]_{IJ}^{\theta_iw_i} = -\int_0^{\overline{r}_i}\varrho_4^{2i-2}\phi_I^{\theta_i}\phi_{J,\xi_i}^{w_i}\,\mathrm{d}\xi_i, \tag{A.1g}$$

$$\left[\overline{\mathbf{K}}_b^T\right]_{IJ}^{\theta_i\theta_i} = \int_0^{\overline{r}_i}\left(\begin{array}{l}\varrho_4^{2i-2}\phi_I^{\theta_i}\phi_J^{\theta_i} + \eta\varrho_3^{2i-2}\phi_{I,\xi_i}^{\theta_i}\phi_{J,\xi_i}^{\theta_i}\\ \quad + \overline{K}_r^T\left(\phi_I^{\theta_i}\phi_J^{\theta_i} + \mu_i^{\,2}\phi_{I,\xi_i}^{\theta_i}\phi_{J,\xi_i}^{\theta_i}\right)\end{array}\right)\mathrm{d}\xi_i, \tag{A.1h}$$

$$\left[\overline{\mathbf{K}}_b^T\right]_{IJ}^{w_iw_j} = -\int_0^{\overline{r}_i}\int_0^{\overline{\Lambda}_i}\overline{C}_{vdW}^T\phi_I^{w_i}\phi_J^{w_j}\,\mathrm{d}\xi_i\,\mathrm{d}\xi_j; \quad i \neq j. \tag{A.1i}$$

A.2. The submatrices associated with the NHOBT

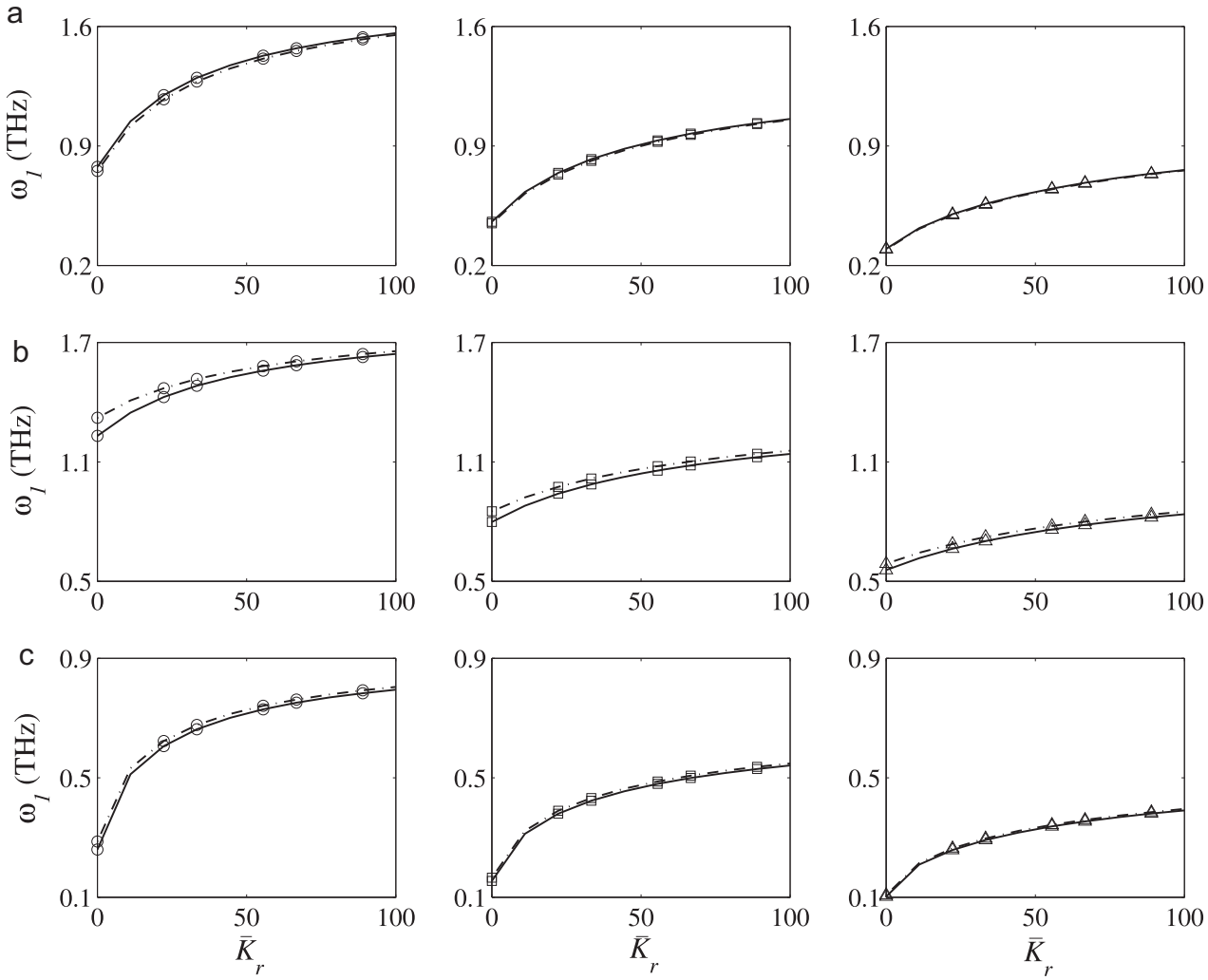

Fig. 12. Effect of the rotational stiffness of the elastic matrix on the fundamental frequency of the nanosystem for various boundary conditions: (a) SS, (b) CC, and (c) CF ((○) $\lambda_1=15$, (□) $\lambda_1=20$, (△) $\lambda_1=25$; e_0a = 1 nm).

$$\overline{\mathbf{w}}_i^H = < \overline{w}_{i_1}^H, \overline{w}_{i_2}^H, \ldots, \overline{w}_{i_{NP_i}}^H >^T ; \quad i, j = 1, 2, \tag{A.2a}$$

$$\overline{\mathbf{\Psi}}_i^H = \langle \overline{\psi}_{i_1}^H, \overline{\psi}_{i_2}^H, \ldots, \overline{\psi}_{i_{NP_i}}^H \rangle^T, \tag{A.2b}$$

$$\left[\overline{\mathbf{M}}_b^H\right]_{IJ}^{\psi_i\psi_i} = \int_0^{\overline{\lambda}_i} \vartheta_7^{2i-2}\left(\phi_I^{\psi_i}\phi_J^{\psi_i} + {\mu_i}^2\phi_{I,\xi_i}^{\psi_i}\phi_{J,\xi_i}^{\psi_i}\right)\mathrm{d}\xi_i, \tag{A.2c}$$

$$\left[\overline{\mathbf{M}}_b^H\right]_{IJ}^{\psi_i w_i} = -\int_0^{\overline{\lambda}_i} \vartheta_2^{2i-2}\gamma_6^2\left(\phi_I^{\psi_i}\phi_{J,\xi_i}^{w_i} + {\mu_i}^2\phi_{I,\xi_i}^{\psi_i}\phi_{J,\xi_i\xi_i}^{w_i}\right)\mathrm{d}\xi_i, \tag{A.2d}$$

$$\left[\overline{\mathbf{M}}_b^H\right]_{IJ}^{w_i w_i} = \int_0^{\overline{\lambda}_i} \begin{pmatrix} \vartheta_1^{2i-2}\left(\phi_I^{w_i}\phi_J^{w_i} + {\mu_i}^2\phi_{I,\xi_i}^{w_i}\phi_{J,\xi_i}^{w_i}\right) + \\ \vartheta_3^{2i-2}\gamma_2^2\left(\phi_{I,\xi_i}^{w_i}\phi_{J,\xi_i}^{w_i} + {\mu_i}^2\phi_{I,\xi_i\xi_i}^{w_i}\phi_{J,\xi_i\xi_i}^{w_i}\right) \end{pmatrix}\mathrm{d}\xi_i, \tag{A.2e}$$

$$\left[\overline{\mathbf{M}}_b^H\right]_{IJ}^{w_i\psi_i} = -\int_0^{\overline{\lambda}_i} \vartheta_2^{2i-2}\gamma_1^2\left(\phi_{I,\xi_i}^{w_i}\phi_J^{\psi_i} + {\mu_i}^2\phi_{I,\xi_i\xi_i}^{w_i}\phi_{J,\xi_i}^{\psi_i}\right)\mathrm{d}\xi_i, \tag{A.2f}$$

$$\left[\overline{\mathbf{K}}_b^H\right]_{IJ}^{w_i w_i} = \int_0^{\overline{\lambda}_i} \begin{pmatrix} \vartheta_4^{2i-2}\gamma_3^2\phi_{I,\xi_i}^{w_i}\phi_{J,\xi_i}^{w_i} + \vartheta_6^{2i-2}\phi_{I,\xi_i\xi_i}^{w_i}\phi_{J,\xi_i\xi_i}^{w_i} + \\ \overline{K}_t^H\left(\phi_I^{w_i} - {\mu_i}^2\phi_{I,\xi_i\xi_i}^{w_i}\right)\phi_J^{w_i} + \\ \int_0^{\overline{\Gamma}_i}\overline{C}_{vdW}^H\left(\phi_I^{w_i} - {\mu_i}^2\phi_{I,\xi_i\xi_i}^{w_i}\right)\phi_J^{w_i}\,\mathrm{d}\xi_{3-i} \end{pmatrix}\mathrm{d}\xi_i, \tag{A.2g}$$

$$\left[\overline{\mathbf{K}}_b^H\right]_{IJ}^{w_i\psi_i} = \int_0^{\overline{\lambda}_i}\left(\vartheta_4^{2i-2}\gamma_3^2\phi_{I,\xi_i}^{w_i}\phi_J^{\psi_i} - \vartheta_5^{2i-2}\gamma_4^2\phi_{I,\xi_i\xi_i}^{w_i}\phi_{J,\xi_i}^{\psi_i}\right)\mathrm{d}\xi_i, \tag{A.2h}$$

$$\left[\overline{\mathbf{K}}_b^H\right]_{IJ}^{\psi_i w_i} = \int_0^{\overline{\lambda}_i}\left(\vartheta_4^{2i-2}\gamma_7^2\phi_I^{\psi_i}\phi_{J,\xi_i}^{w_i} - \vartheta_5^{2i-2}\gamma_9^2\phi_{I,\xi_i}^{w_i}\phi_{J,\xi_i\xi_i}^{w_i}\right)\mathrm{d}\xi_i, \tag{A.2i}$$

$$\left[\overline{\mathbf{K}}_b^H\right]_{IJ}^{\psi_i\psi_i} = \int_0^{\overline{\lambda}_i} \begin{pmatrix} \vartheta_4^{2i-2}\gamma_7^2\phi_I^{\psi_i}\phi_J^{\psi_i} + \vartheta_8^{2i-2}\gamma_8^2\phi_{I,\xi_i}^{\psi_i}\phi_{J,\xi_i}^{\psi_i} + \\ \overline{K}_r^H\left(\phi_I^{\psi_i} - {\mu_i}^2\phi_{I,\xi_i\xi_i}^{\psi_i}\right)\phi_J^{\psi_i} \end{pmatrix}\mathrm{d}\xi_i, \tag{A.2j}$$

$$\left[\overline{\mathbf{K}}_b^H\right]_{IJ}^{w_i w_j} = -\int_0^{\overline{\lambda}_i}\int_0^{\overline{\Gamma}_i}\overline{C}_{vdW}^H\phi_I^{w_i}\phi_J^{w_j}\mathrm{d}\xi_i\,\mathrm{d}\xi_j; \quad i \neq j. \tag{A.2k}$$

Appendix B. Frequency analysis of the elastically embedded

DPSWCNTs via AMM

In AMM analysis of structures, the unknown deformation fields are expressed as a function of admissible mode shapes. These modes are obtainable from free vibration equations of motion and they should satisfy at least the essential boundary conditions of the problem. Commonly, Galerkin method in conjunction with these admissible modes is exploited to determine the unknown fields of the problem. Herein, in order to magnify the accuracy of the AMM analysis, we use the advantages of using the integration by parts. To this end, we replace the shape functions given in the mass and stiffness matrices of Appendices A.1 and A.2 by the appropriate mode shapes.

B.1. Free transverse vibration of the nanosystem on the basis of the NTBT using AMM

For a simply supported DPSWCNTs surrounded by an elastic medium, the dimensionless transverse displacement and angle of deformation can be stated by

$$\overline{w}_i^T(\xi_i,\tau)=\sum_{k=1}^{NM_i}\phi_k^{w_i}(\xi_i)\overline{w}_{ik}^T(\tau),\quad \overline{\theta}_i^T(\xi_i,\tau)=\sum_{k=1}^{NM_i}\phi_k^{\theta_i}(\xi_i)\overline{\theta}_{ik}^T(\tau);\ \ i=1,2, \tag{B.1}$$

where $\phi_k^{w_i}(\xi_i)=\sqrt{2}\sin(k\pi\xi_i)$ and $\phi_k^{\theta_i}(\xi_i)=\sqrt{2}\cos(k\pi\xi_i)$ represent the kth mode shapes associated with the transverse displacement and angle of deformation fields of the ith simply supported nanotube, respectively. By substituting these vibration modes into Eqs. (A.1c)–(A.1i), the mass and stiffness submatrices are obtained as follows:

$$\left[\overline{\mathbf{M}}_b^T\right]_{kl}^{w_iw_i}=\varrho_1^{2i-2}\left(1+kl(\mu\pi)^2\right)\delta_{kl}, \tag{B.2a}$$

$$\left[\overline{\mathbf{M}}_b^T\right]_{kl}^{\theta_i\theta_i}=\lambda_1^{-2}\varrho_2^{2i-2}\left(1+kl(\mu\pi)^2\right)\delta_{kl}, \tag{B.2b}$$

$$\left[\overline{\mathbf{K}}_b^T\right]_{kl}^{w_iw_i}=\left(kl\pi^2\,\varrho_4^{2i-2}+\left(1+(\mu\pi k)^2\right)\overline{K}_t^T\right)\delta_{kl}+\int_0^{\overline{\Gamma}_i}\int_0^{\overline{\Lambda}_i}\overline{C}_{vdW}^T\left(\phi_k^{w_i}-\mu_i^2\phi_{k,\xi_i\xi_i}^{w_i}\right)\phi_l^{w_i}\,\mathrm{d}\xi_{3-i}\,\mathrm{d}\xi_i, \tag{B.2c}$$

$$\left[\overline{\mathbf{K}}_b^T\right]_{kl}^{w_i\theta_i}=-k\pi\delta_{kl}, \tag{B.2d}$$

$$\left[\overline{\mathbf{K}}_b^T\right]_{kl}^{\theta_iw_i}=-l\pi\delta_{kl}, \tag{B.2e}$$

$$\left[\overline{\mathbf{K}}_b^T\right]_{kl}^{\theta_i\theta_i}=\left(\varrho_4^{2i-2}+\eta\varrho_3^{2i-2}kl\pi^2+kl\left(1+(\mu\pi)^2\right)\overline{K}_r^T\right)\delta_{kl}, \tag{B.2f}$$

$$\left[\overline{\mathbf{K}}_b^T\right]_{kl}^{w_iw_j}=-\int_0^{\overline{\Gamma}_i}\int_0^{\overline{\Lambda}_i}\overline{C}_{vdW}^T\,\phi_k^{w_i}\phi_l^{w_j}\mathrm{d}\xi_i\,\mathrm{d}\xi_j;\quad i\neq j. \tag{B.2g}$$

B.2. Free transverse vibration of the nanosystem on the basis of the NHOBT using AMM

For a simply supported DPSWCNTs embedded in an elastic matrix on the basis of the NHOBT, the dimensionless deformation fields are expressed by

$$\overline{w}_i^H(\xi_i,\tau)=\sum_{k=1}^{NM_i}\phi_k^{w_i}(\xi_i)\overline{w}_{ik}^H(\tau),\ \overline{\psi}_i^H(\xi_i,\tau)=\sum_{k=1}^{NM_i}\phi_k^{\psi_i}(\xi_i)\overline{\psi}_{ik}^H(\tau);\quad i=1,2 \tag{B.3}$$

where $\phi_k^{w_i}(\xi_i)=\sqrt{2}\sin(k\pi\xi_i)$ and $\phi_k^{\psi_i}(\xi_i)=\sqrt{2}\cos(k\pi\xi_i)$. By substituting these mode shapes into Eqs. (A.2c)–(A.2k), one can arrive at the following relations:

$$\left[\overline{\mathbf{M}}_b^H\right]_{kl}^{\psi_i\psi_i}=\vartheta_7^{2i-2}\left(1+kl(\mu\pi)^2\right)\delta_{kl}, \tag{B.4a}$$

$$\left[\overline{\mathbf{M}}_b^H\right]_{kl}^{\psi_iw_i}=-\vartheta_2^{2i-2}\gamma_6^2k\pi\left(1+(\mu\pi l)^2\right)\delta_{kl}, \tag{B.4b}$$

$$\left[\overline{\mathbf{M}}_b^H\right]_{kl}^{w_iw_i}=\left(1+(\mu\pi kl)^2\right)\left(\vartheta_1^{2i-2}+\vartheta_3^{2i-2}(\pi kl\gamma_2)^2\right)\delta_{kl}, \tag{B.4c}$$

$$\left[\overline{\mathbf{M}}_b^H\right]_{kl}^{w_i\psi_i}=-\vartheta_2^{2i-2}\gamma_1k\pi\left(1+(\mu\pi)^2kl\right)\delta_{kl}, \tag{B.4d}$$

$$\left[\overline{\mathbf{K}}_b^H\right]_{kl}^{w_iw_i}=\left(\vartheta_4^{2i-2}\gamma_3^2\pi^2kl+\vartheta_6^{2i-2}\pi^4k^2l^2+\left(1+(\mu\pi k)^2\right)\overline{K}_t^H\right)\delta_{kl}+\int_0^{\overline{\Gamma}_i}\int_0^{\overline{\Lambda}_i}\overline{C}_{vdW}^T\left(\phi_k^{w_i}-\mu_i^2\phi_{k,\xi_i\xi_i}^{w_i}\right)\phi_l^{w_i}\,\mathrm{d}\xi_{3-i}\,\mathrm{d}\xi_i, \tag{B.4e}$$

$$\left[\overline{\mathbf{K}}_b^H\right]_{kl}^{w_i\psi_i}=k\pi\left(\vartheta_4^{2i-2}\gamma_3^2-kl\pi^2\vartheta_5^{2i-2}\gamma_4^2\right)\delta_{kl}, \tag{B.4f}$$

$$\left[\overline{\mathbf{K}}_b^H\right]_{kl}^{\psi_iw_i}=l\pi\left(\vartheta_4^{2i-2}\gamma_7^2-kl\pi^2\vartheta_5^{2i-2}\gamma_9^2\right)\delta_{kl}, \tag{B.4g}$$

$$\left[\overline{\mathbf{K}}_b^H\right]_{kl}^{\psi_i\psi_i}=\left(\vartheta_4^{2i-2}\gamma_7^2+kl\pi^2\vartheta_8^{2i-2}\gamma_8^2+\overline{K}_r^H\left(1+kl(\mu\pi)^2\right)\right)\delta_{kl}, \tag{B.4h}$$

$$\left[\overline{\mathbf{K}}_b^H\right]_{kl}^{w_iw_j}=-\int_0^{\overline{\Gamma}_i}\int_0^{\overline{\Lambda}_i}\overline{C}_{vdW}^H\phi_k^{w_i}\phi_l^{w_j}\mathrm{d}\xi_i\,\mathrm{d}\xi_j;\quad i\neq j. \tag{B.4i}$$

References

[1] D. Cai, J.M. Mataraza, Z.H. Qin, Z. Huang, J. Huang, T.C. Chiles, D. Carnahan, K. Kempa, Z. Ren, Highly efficient molecular delivery into mammalian cells using carbon nanotube spearing, Nat. Methods 2 (6) (2005) 449–454.

[2] R. Singh, D. Pantarotto, D. McCarthy, O. Chaloin, J. Hoebeke, C.D. Partidos, J. P. Briand, M. Prato, A. Bianco, K. Kostarelos, Binding and condensation of plasmid DNA onto functionalized carbon nanotubes: toward the construction of nanotube-based gene delivery vectors, J. Am. Chem. Soc. 127 (12) (2005) 4388–4396.

[3] A.A. Bhirde, P. Vyomesh, J. Gavard, G. Zhang, A.A. Sousa, A. Masedunskas, R. D. Leapman, R. Weigert, J.S. Gutkind, J.F. Rusling, Targeted killing of cancer cells in vivo and in vitro with EGF-directed carbon nanotube-based drug delivery, ACS Nano 3 (2) (2009) 307–316.

[4] I. Robel, B.A. Bunker, P.V. Kamat, Single-walled carbon nanotube-CdS nanocomposites as light-harvesting assemblies: photoinduced charge-transfer interactions, Adv. Mater. 17 (20) (2005) 2458–2463.

[5] R. Hu, B.A. Cola, N. Haram, J.N. Barisci, S. Lee, S. Stoughton, G. Wallace, et al., Harvesting waste thermal energy using a carbon-nanotube-based thermoelectrochemical cell, Nano Lett. 10 (3) (2010) 838–846.

[6] K. Jensen, C. Girit, W. Mickelson, A. Zettl, Tunable nanoresonators constructed from telescoping nanotubes, Phys. Rev. Lett. 96 (21) (2006) 215503.

[7] M. Jie, L. Li, Frequency self-tuning of carbon nanotube resonator with application in mass sensors, Sens. Actuat. B Chem. 188 (2013) 661–668.

[8] H. Pathangi, V. Cherman, A. Khaled, B. Soree, G. Groeseneken, A. Witvrouw, Towards CMOS-compatible single-walled carbon nanotube resonators, Microelectron. Eng. 107 (2013) 219–222.

[9] Q. Wang, B. Arash, A review on applications of carbon nanotubes and graphenes as nano-resonator sensors, Comput. Mater. Sci. 82 (2014) 350–360.

[10] S. Tung, H. Rokadia, W.J. Li, A microshear stress sensor based on laterally aligned carbon nanotubes, Sens. Actuat. A Phys. 133 (2) (2007) 431–438.

[11] S. Dhall, N. Jaggi, R. Nathawat, Functionalized multiwalled carbon nanotubes based hydrogen gas sensor, Sens. Actuat. A Phys. 201 (2013) 321–327.

[12] P. Qi, O. Vermesh, M. Grecu, A. Javey, Q. Wang, H. Dai, S. Peng, K.J. Cho, Toward large arrays of multiplex functionalized carbon nanotube sensors for highly sensitive and selective molecular detection, Nano Lett. 3 (3) (2003) 347–351.

[13] B. Ashrafi, P. Hubert, S. Vengallatore, Carbon nanotube-reinforced composites as structural materials for microactuators in microelectromechanical systems, Nanotechnology 17 (19) (2006) 4895.
[14] W. Fang, H.Y. Chu, W.K. Hsu, T.W. Cheng, N.H. Tai, Polymer-Reinforced, Aligned multiwalled carbon nanotube composites for microelectromechanical systems applications, Adv. Mater. 17 (24) (2005) 2987–2992.
[15] V. Sazonova, Y. Yaish, H. Ustunel, D. Roundy, T.A. Arias, P.L. McEuen, A tunable carbon nanotube electromechanical oscillator, Nature 431 (7006) (2004) 284–287.
[16] Q. Wang, V.K. Varadan, Vibration of carbon nanotubes studied using nonlocal continuum mechanics, Smart Mater. Struct. 15 (2) (2006) 659.
[17] J.N. Reddy, S.D. Pang, Nonlocal continuum theories of beams for the analysis of carbon nanotubes, J. Appl. Phys. 103 (2) (2008) 023511.
[18] K. Kiani, A nonlocal meshless solution for flexural vibrations of double-walled carbon nanotubes, Appl. Math. Comput. 234 (2014) 557–578.
[19] K. Kiani, B. Mehri, Assessment of nanotube structures under a moving nanoparticle using nonlocal beam theories, J. Sound Vib. 329 (11) (2010) 2241–2264.
[20] M. Simsek, Nonlocal effects in the forced vibration of an elastically connected double-carbon nanotube system under a moving nanoparticle, Comput. Mater. Sci. 50 (7) (2011) 2112–2123.
[21] K. Kiani, Nanoparticle delivery via stocky single-walled carbon nanotubes: a nonlinear-nonlocal continuum-based scrutiny, Compos. Struct. 116 (2014) 254–272.
[22] K. Kiani, Nonlinear vibrations of a single-walled carbon nanotube for delivering of nanoparticles, Nonlinear Dyn. 76 (4) (2014) 1885–1903.
[23] H.L. Lee, W.J. Chang, Free transverse vibration of the fluid-conveying single-walled carbon nanotube using nonlocal elastic theory, J. Appl. Phys. 103 (2) (2008) 024302.
[24] L. Wang, Dynamical behaviors of double-walled carbon nanotubes conveying fluid accounting for the role of small length scale, Comput. Mater. Sci. 45 (2) (2009) 584–588.
[25] K. Kiani, Nanofluidic flow-induced longitudinal and transverse vibrations of inclined stocky single-walled carbon nanotubes, Comput. Methods Appl. Mech. Eng. 276 (2014) 691–723.
[26] Z.B. Shen, X.F. Li, L.P. Sheng, G.J. Tang, Transverse vibration of nanotube-based micro-mass sensor via nonlocal Timoshenko beam theory, Comput. Mater. Sci. 53 (1) (2012) 340–346.
[27] T. Murmu, S. Adhikari, Nonlocal frequency analysis of nanoscale biosensors, Sens. Actuat. A Phys. 173 (1) (2012) 41–48.
[28] A.M. Patel, A.Y. Joshi, Investigating the influence of surface deviations in double walled carbon nanotube based nanomechanical sensors, Comput. Mater. Sci. 89 (15) (2014) 157–164.
[29] K. Kiani, Vertically aligned carbon nanotubes for sensing unidirectional fluid flow, Physica B (2015), http://dx.doi.org/10.1016/j.physb.2015.01.033.
[30] X. Wang, J.X. Shen, Y. Liu, G.G. Shen, G. Lu, Rigorous van der Waals effect on vibration characteristics of multi-walled carbon nanotubes under a transverse magnetic field, Appl. Math. Model. 36 (2) (2012) 648–656.
[31] T. Murmu, M.A. McCarthy, S. Adhikari, Vibration response of double-walled carbon nanotubes subjected to an externally applied longitudinal magnetic field: a nonlocal elasticity approach, J. Sound Vib. 331 (23) (2012) 5069–5086.
[32] K. Kiani, Longitudinally varying magnetic field influenced transverse vibration of embedded double-walled carbon nanotubes, Int. J. Mech. Sci. 87 (2014) 179–199.
[33] L.L. Ke, Y. Xiang, J. Yang, S. Kitipornchai, Nonlinear free vibration of embedded double-walled carbon nanotubes based on nonlocal Timoshenko beam theory, Comput. Mater. Sci. 47 (2) (2009) 409–417.
[34] Y.Z. Wang, F.M. Li, Nonlinear free vibration of nanotube with small scale effects embedded in viscous matrix, Mech. Res. Commun. 60 (2014) 45–51.
[35] K.Y. Xu, X.N. Guo, C.Q. Ru, Vibration of a double-walled carbon nanotube aroused by nonlinear intertube van der Waals forces, J. Appl. Phys. 99 (6) (2006) 064303.
[36] K. Kiani, Nonlocal continuous models for forced vibration analysis of two- and three-dimensional ensembles of single-walled carbon nanotubes, Physica E 60 (2014) 229–245.
[37] K. Kiani, In- and out-of- plane dynamic flexural behaviors of two-dimensional ensembles of vertically aligned single-walled carbon nanotubes, Physica B 449 (2014) 164–180.
[38] K. Kiani, Nonlocal discrete and continuous modeling of free vibration of stocky ensembles of single-walled carbon nanotubes, Curr. Appl. Phys. 14 (8) (2014) 1116–1139.
[39] T. Murmu, S. Adhikari, Nonlocal transverse vibration of double-nanobeam-systems, J. Appl. Phys. 108 (8) (2010) 083514(1–9).
[40] T. Murmu, M.A. McCarthy, S. Adhikari, Nonlocal elasticity based magnetic field affected vibration response of double single-walled carbon nanotube systems, J. Appl. Phys. 111 (11) (2012) 113511.
[41] A.C. Eringen, Nonlocal polar elastic continua, Int. J. Eng. Sci. 10 (1) (1972) 1–16.
[42] A.C. Eringen, C.G. Speziale, B.S. Kim, Crack-tip problem in non-local elasticity, J. Mech. Phys. Solids 25 (5) (1977) 339–355.
[43] A.C. Eringen, Nonlocal Continuum Field Theories, Springer-Verlag, NY, 2002.
[44] S.P. Timoshenko, On the correction for shear of the differential equation for transversevibrations of prismatic bars, Philos. Mag. 41 (1921) 744–746.
[45] S.P. Timoshenko, On the transverse vibrations of bars of uniform cross-section, Philos. Mag. 43 (1922) 125–131.
[46] J.N. Reddy, A simple higher-order theory for laminated composite plates, J. Appl. Mech. 51 (1984) 745–752.
[47] W.B. Bickford, A consistent higher order beam theory, Dev. Theor. Appl. Mech. 11 (1982) 137–150.
[48] S.S. Gupta, R.C. Batra, Continuum structures equivalent in normal mode vibrations to single-walled carbon nanotubes, Comput. Mater. Sci. 43 (4) (2008) 715–723.
[49] S.S. Gupta, F.G. Bosco, R.C. Batra, Wall thickness and elastic moduli of single-walled carbon nanotubes from frequencies of axial, torsional and inextensional modes of vibration, Comput. Mater. Sci. 47 (4) (2010) 1049–1059.
[50] J.E. Lennard-Jones, The determination of molecular fields: from the variation of the viscosity of a gas with temperature, Proc. R. Soc. Lond. Ser. A 106 (1924) 441–462.
[51] G.J. Wagner, W.K. Liu, Application of essential boundary conditions in mesh-free methods: a corrected collocation method, Int. J. Numer. Methods Eng. 47 (8) (2000) 1367–1379.
[52] J.N. Reddy, Nonlocal theories for bending, buckling and vibration of beams, Int. J. Eng. Sci. 45 (2) (2007) 288–307.